Available online at www.sciencedirect.com

ScienceDirect

Geochimica et Cosmochimica Acta 191 (2016) 216–238

Geochimica et Cosmochimica Acta

www.elsevier.com/locate/gca

Water in volcanic glass: From volcanic degassing to secondary hydration

Angela N. Seligman *, Ilya N. Bindeman, James M. Watkins, Abigail M. Ross

Department of Geological Sciences, 1272 University of Oregon, Eugene, OR 97403-1272, USA

Received 3 December 2015; accepted in revised form 10 July 2016; available online 25 July 2016

Abstract

Volcanic glass is deposited with trace amounts (0.1–0.6 wt.%) of undegassed magmatic water dissolved in the glass. After deposition, meteoric water penetrates into the glass structure mostly as molecular H_2O. Due to the lower δD (‰) values of non-tropical meteoric waters and the ~30‰ offset between volcanic glass and environmental water during hydration, secondary water imparts lighter hydrogen isotopic values during secondary hydration up to a saturation concentration of 3–4 wt.% H_2O. We analyzed compositionally and globally diverse volcanic glass from 0 to 10 ka for their δD and H_2O_t across different climatic zones, and thus different δD of precipitation, on a thermal conversion elemental analyzer (TCEA) furnace attached to a mass spectrometer. We find that tephrachronologically coeval rhyolite glass is hydrated faster than basaltic glass, and in the majority of glasses an increase in age and total water content leads to a decrease in δD (‰), while a few equatorial glasses have little change in δD (‰). We compute a magmatic water correction based on our non-hydrated glasses, and calculate an average $10^3\ln\alpha_{glass\text{-}water}$ for our hydrated felsic glasses of −33‰, which is similar to the $10^3\ln\alpha_{glass\text{-}water}$ determined by Friedman et al. (1993a) of −34‰. We also determine a smaller average $10^3\ln\alpha_{glass\text{-}water}$ for all our mafic glasses of −23‰. We compare the δD values of water extracted from our glasses to local meteoric waters following the inclusion of a −33‰ $10^3\ln\alpha_{glass\text{-}water}$. We find that, following a correction for residual magmatic water based on an average δD and wt.% H_2O_t of recently erupted ashes from our study, the δD value of water extracted from hydrated volcanic glass is, on average, within 4‰ of local meteoric water. To better understand the difference in hydration rates of mafic and felsic glasses, we imaged 6 tephra clasts ranging in age and chemical composition with BSE (by FEI SEM) down to a submicron resolution. Mafic tephra have more bubbles per unit area (25–77 mm^{-2}) than felsic tephra (736 mm^{-2}) and thicker average bubble walls (0.07 mm) than felsic tephra (0.02 mm). We use a simplified diffusion model to quantify the hydration rate of vesicular glass as a function of the diffusivity of water and the average bubble wall thickness. Based on fits to our hydration rate data, we estimate the initial low-temperature diffusivity at 0.1 wt.% H_2O_t in volcanic glass (mafic and felsic) to be on the order of 10^{-3} to 10^{-4} μm^2/year and find that differences in hydration rates between mafic and felsic tephra can be attributed primarily to differences in vesicularity, although slightly slower hydration of basalt cannot be precluded. We also observe no consistent temporal difference in secondary meteoric water uptake in wet versus dry and hot versus cold climates.

Keywords: Secondary hydration; Hydrogen isotopes; Diffusion; Water; Paleoenvironments; Kamchatka

* Corresponding author.
E-mail addresses: seligman@uoregon.edu (A.N. Seligman), bindeman@uoregon.edu (I.N. Bindeman), watkins4@uoregon.edu (J.M. Watkins), aross4@uoregon.edu (A.M. Ross).

http://dx.doi.org/10.1016/j.gca.2016.07.010
0016-7037/

1. INTRODUCTION

Volcanic glass is widely used for paleoclimate studies due to its uptake of meteoric water following deposition (Friedman et al., 1993b). This process is also known as secondary hydration or 'rehydration'. The presence of environmental waters in volcanic glass has been used as a tracer of the δD of local precipitation at the time of deposition (e.g. Riciputi et al., 2002; Mulch et al., 2007; Cassel et al., 2014; Canavan et al., 2014), and the extent of hydration by meteoric waters has been used to estimate the age of obsidian artifacts (e.g. Friedman et al., 1966; Anovitz et al., 2004). However, volcanic glass can be deposited with unknown quantities of primary magmatic water, which varies as a consequence of magmatic degassing processes (Newman et al., 1988; Dobson et al., 1989; Castro et al., 2014). Both magmatic and meteoric water can have distinct δD values (e.g. DeGroat-Nelson et al., 2001; Tuffen et al., 2010), depending on the δD value of the meteoric water that is diffusing into the glass, the degree of volcanic degassing that has occurred, and the original δD of the parental undegassed magma (Figs. 1 and 2). Therefore, these two types of water can obscure each other in δD-H_2O space when they are both present in volcanic glass, even though they could both provide useful information if the properties of one can be known or constrained. Furthermore, the details of secondary hydration are not well understood, and it is still unknown how long it takes for mafic and felsic glass to become secondarily hydrated at surface temperature and pressure.

1.1. Secondary hydration of volcanic glass

Rehydration of degassed (primarily water-free) silicate glass is a complex process of interface kinetics, water in-diffusion, and possibly minor re-speciation of hydrogen between dissolved molecular water and hydroxyl groups (e.g. Zhang, 1999; Anovitz et al., 2008; Nolan and Bindeman, 2013). The proposed models for rehydration range from a simple linear increase to a square root of time dependence (e.g. Friedman et al., 1966; Nolan and Bindeman, 2013 and references therein). Since the diffusion coefficients of water in glass are a strong function of water concentration (Zhang and Behrens, 2000), hydration proceeds with a 'hydration front' that has a relatively sharp interface, which is possible to observe under a microscope (Ross and Smith, 1955; Friedman et al., 1966) and has therefore been used as a chronometer for dating. Riciputi et al. (2002) used microscopic observations and SIMS depth profiling of ancient obsidian artifacts of known age to quantify the distance of the hydration front 'X' into volcanic glass and determined that this distance (X) is proportional to the sum of linear and square root terms evaluated at time (t) (e.g. Friedman et al., 1966; Anovitz et al., 2004):

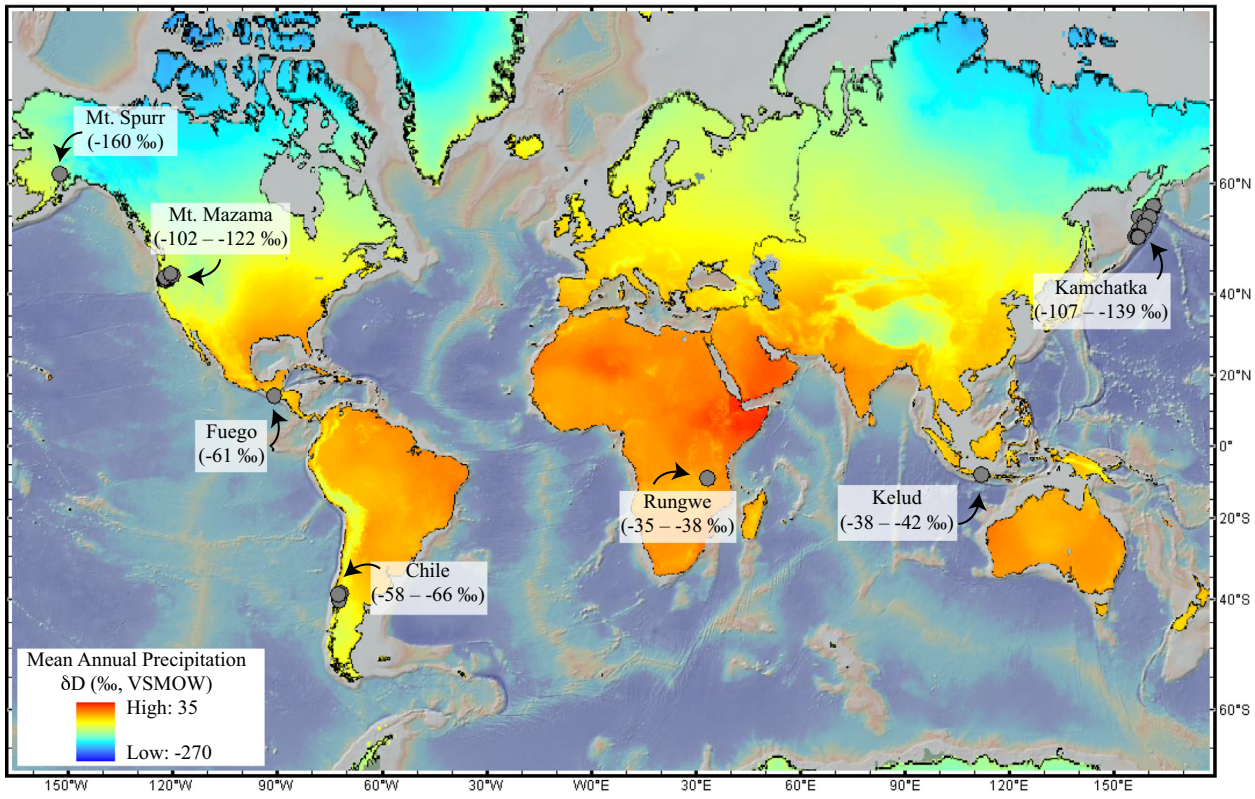

Fig. 1. Sample locations along with local δD of precipitation range in ‰ plotted on a world map with an overlay of δD values (‰) of current precipitation (Bowen and Revenaugh, 2003; Bowen, 2015). The map was created using GeoMapApp as the underlying base map (the Global Multi-Resolution Topography (GMRT) synthesis). GPS coordinates and local δD (‰) of precipitation values for sample locations can be found in Table 1.

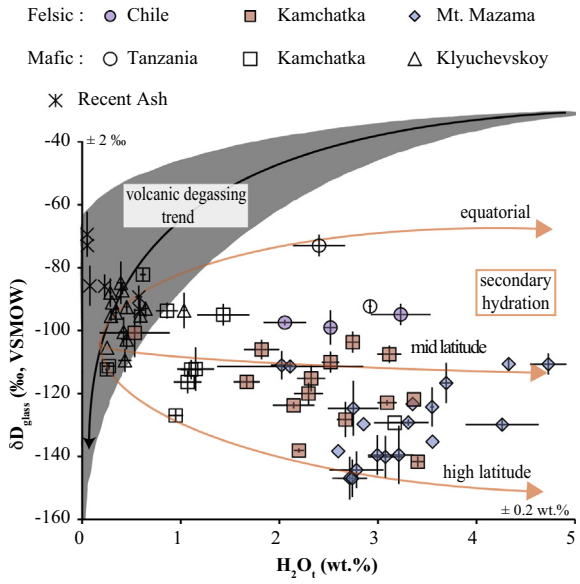

Fig. 2. δD_{glass} in relation to the total concentration of water extracted from the glass (error bars illustrate ± 1 s.d.). Two separate trends are shown: (1) The relationship between the δD (‰) and H_2O_t (wt.%) of volcanic degassing from Newman et al. (1988) and Castro et al. (2014) showing a decrease in δD (‰) with a decrease in total water concentration in the glass. The volcanic degassing trend illustrates the wide range in δD values for magmatic waters worldwide, with a trend towards heavier δD values at higher water concentrations; and (2) The relationship between the δD (‰) and H_2O_t (wt.%) of secondary hydration, which generally shows a decrease in δD (‰) with an increase in total water concentration in the glass. Although these trends are opposite one another, there is an overlap in δD (‰) values at water concentrations below ~1 wt.% H_2O_t between volcanic degassing and secondary hydration of volcanic glass. Otherwise, values above ~1 wt.% H_2O_t and below ~−70‰ δD signify secondary hydration for non-tropical samples, while heavier δD (‰) values signify volcanic degassing and the presence of mostly primary magmatic water. This is based on the typical lower δD (‰) of precipitation in comparison to the δD (‰) of magmatic water. Local δD of precipitation for the locations where our glass samples were collected range between −35 and −160‰ (Fig. 1). The ±2‰ δD and ±0.2 wt.% H_2O_t on each axis illustrate the typical reproducibility of our TCEA.

$$X \sim at + b\sqrt{Dt} \quad (1)$$

where a and b are coefficients that depend on glass composition and climate, and D is a water concentration-dependent diffusion coefficient.

Secondary hydration of rhyolitic glass at ambient temperature and pressure is thought to occur first through the exchange of hydrogen and deuterium ions with water soluble ions such as Na^+, K^+, and Ca^{2+} and then by the absorption of H_2O_{mol} (molecular H_2O) (Jezek and Noble, 1978; Cerling et al., 1985; Oelkers, 2001; Rébiscoul et al., 2007; Valle et al., 2010). In contrast, alteration of basaltic glass leads to the formation of palagonite-rich areas (~10 wt.% water) on the outer rind of the glass (Stroncik and Schmincke, 2002; Crovisier et al., 2003; Parruzot et al., 2015). Although the hydration of mafic and felsic glass is different in some ways, previous work by Crovisier et al. (2003), Cailleteau et al. (2008) and Valle et al. (2010) showed that during the process of secondary hydration of both mafic and felsic volcanic glass, a thin (nanometers to micrometers, depending on time) layer of maximally (4–5 wt.% H_2O_t) hydrated glass, or 'gel layer', is formed on the surface of the glass. Increased densification, which leads to the closure of pores, causes the gel layer to serve as a protective film, which decreases the rate of further hydration of the glass interior. The formation of a gel layer is essential for studies involving nuclear waste disposal, but a decrease, instead of a cessation, of alteration or hydration can still be problematic for paleoenvironmental research that utilizes hydrogen isotopes, as was demonstrated by Anovitz et al. (2009) and Nolan and Bindeman (2013).

1.2. Hydrogen isotopes in secondarily hydrated volcanic glass

Friedman et al. (1966, 1993b) first proposed that hydrogen isotopes in secondarily hydrated ash and pumice could be used as a tool to monitor the D/H of the original hydrating water. Friedman et al. (1993a) showed that water uptake during rehydration results in an approximately −29 to −31‰ offset between felsic glass and water (the glass being isotopically lighter). Their experiments led to a semi-empirical fractionation factor of $\alpha_{glass\text{-}water} = 0.9668 \pm 0.0005$ ($10^3 \ln\alpha_{glass\text{-}water}$ of −34‰). Subsequent research (e.g. Shane and Ingraham, 2002; Mulch et al., 2007; Cassel et al., 2014; Dettinger and Quade, 2015) has demonstrated that this empirically derived fractionation factor does not vary significantly across different surface level climatic conditions.

Recent studies have attempted to determine the reliability of the use of hydrogen isotopes as a paleoenvironmental indicator. Anovitz et al. (2009) used polished obsidian surfaces and isotopically labeled vapors to show that during secondary hydration at elevated temperature (150 °C), primary magmatic water dissolved in volcanic glass exchanges isotopically with secondary water that diffuses into the glass. That is, any hydrogen already dissolved in the glass is not strongly bound to the aluminosilicate matrix and is able to exchange and/or undergo further diffusion into the glass. Subsequently, Nolan and Bindeman (2013) used long-term (3 years) time series experiments at 70, 40, and 20 °C with natural ash from the already secondarily hydrated 7.7 ka Mt. Mazama eruption to show that hydrogen isotopes equilibrate with surrounding deuterated waters on a timescale of years for 70 °C and 40 °C experiments. While hydrogen isotopes were able to readily exchange between ash and surrounding waters, the total water concentration and the $\delta^{18}O$ of the extracted water in the Nolan and Bindeman (2013) experiments remained relatively constant and identical to the original water. These studies by Anovitz et al. (2009) and Nolan and Bindeman (2013) indicate that once ash becomes secondarily hydrated, its hydrogen isotopic ratio may be subject to change.

1.3. Primary versus secondary waters in volcanic glass

When relating D/H and H_2O_t (total water including molecular and hydroxyl groups) in secondarily hydrated tephra to ambient meteoric water, it is important to be able to estimate the residual amounts of (isotopically distinct) primary magmatic water (Fig. 2). Thus, an inherent difficulty exists in determining quantities of residual magmatic water left in volcanic glass, the environmentally-added water, and how to distinguish between these two during analysis. Furthermore, the potential exchange of hydrogen isotopes between the infiltrating secondary waters and the original primary magmatic waters, as well as the changing D/H of secondary waters through time, could further complicate environmental signals.

It is thought that the major difference between magmatic and environmental water is that, at low H_2O_t concentrations, magmatic water is predominantly in the form of dissolved OH^-, whereas environmental water is predominantly H_2O_{mol} (e.g. Newman et al., 1986; Silver et al., 1990; Giachetti et al., 2015). This is due to the higher energy, or temperature, needed for $H_2O_{mol} + O^{2-} = 2OH^-$ respeciation to form SiOH bonds rather than hydrogen bonds that are formed during the addition of H_2O_{mol}. Investigation of water speciation and distinguishing between different water types during progressive degassing creates potential opportunities to distinguish between magmatic and meteoric water (Fig. 3). Giachetti et al. (2015) used the TGA (Thermogravimetric Analysis) technique and compiled data for known water concentrations of 0.0005–22.5 ka intermediate to felsic volcanic glass ranging from approximately 0–4 wt.% H_2O_t to model the rate of secondary hydration of intermediate–felsic volcanic glass. They concluded that, at surface temperatures, intermediate to felsic volcanic glass has a rehydration diffusivity of approximately 10^{-23} m^2 s^{-1} (±approximately one order of magnitude), which is slightly slower than previously determined diffusion rates for nuclear glasses at 50 °C of 10^{-21} m^2 s^{-1} (Ferrand et al., 2006). Giachetti et al. (2015) also numerically modeled TGA outputs to gain further insight into the process of secondary hydration through attempting to distinguish the difference in magmatic and meteoric water in volcanic glass. As with any step heating technique, the assumption is that secondary water (H_2O_{mol}) is released at lower temperatures, while the more strongly bound primary magmatic water (OH^-) is released at higher temperatures. They showed that the 1060 CE Glass Mountain rhyolitic pumices from California contain only small amounts (0.2–0.5 wt.%) of residual primary magmatic water, and had 1–2 wt.% meteoric water. In addition, TGA coupled with FTIR (Fourier Transform Infrared) spectroscopy and D/H determination of hydrous Mt. Mazama ash was used by Nolan and Bindeman (2013) to understand proper heating temperatures to remove the most loosely bound adsorbed water on the glass, and at what temperatures the most tightly bound, possibly magmatic water, is released. These authors observed a progressive increase in OH^-/H_2O_{mol} in the glass during heating and dehydration, which potentially documented the release of secondary meteoric water as H_2O_{mol} with low δD values. Importantly, the δD value of this progressively extracted water did not vary significantly below 600 °C. High OH^-/H_2O_{mol} and higher δD values were observed within the final 0.5 wt.% H_2O_t at the end of step heating (above 600 °C), which is interpreted to be primary magmatic water.

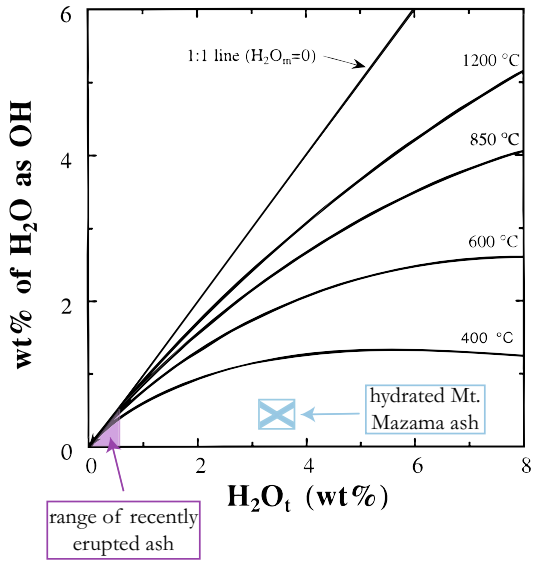

Fig. 3. Relative quantities of H_2O_t and OH^- as modified from Ihinger et al. (1999), illustrating the larger quantities of OH^- relative to total H_2O_{mol} as temperature increases. We include potential ranges of recently erupted ash, which are from this study. We also include the location of secondarily hydrated Mt. Mazama ash from Nolan and Bindeman (2013), illustrating the low OH^- concentration relative to the concentration of H_2O_{mol} for low temperature hydration.

Collectively, these studies demonstrate that it is possible to obtain an estimate of the proportion of primary and secondary water in volcanic glass. It is not currently practical to conduct experiments for measuring the hydration rate of glass at room temperature, due to the very slow rates of secondary hydration (1–10 μm/1000 years; Friedman et al., 1966; this study, see below). Below we attempt to further the understanding of secondary hydration at surface temperatures through the use of hydrogen isotopes, total water concentration, and relative vesicularities by using a natural experiment involving tephra of known ages.

1.4. Goals of the present study

Given the gaps in our understanding of the secondary hydration process, our research questions include:

(1) What is the rate of secondary hydration for mafic and felsic volcanic glass?
(2) What causes the difference in hydration rates between mafic and felsic glass?
(3) How do the isotopes of hydrogen (D/H) behave during secondary hydration?
(4) What effect does the D/H ratio of the residual primary magmatic water have on the D/H ratio of the total water during analyses of volcanic glass?
(5) Is the fractionation between meteoric water and water-in-glass the same for mafic and felsic glasses?

To answer these questions, we use a series of natural volcanic tephra layers of known age across different climates to provide insight into the secondary hydration process in terms of the rates of secondary hydration and its isotopic signature (Table 1, Fig. 1). These volcanic tephra layers from around the world cover a large range of δD_{met} (δD of meteoric water) that also range in age, chemical composition, water concentration (wt.%) and δD (‰). By utilizing volcanic ash and tephra, we gain a wider range of data than would be possible through the use of obsidian artifacts, and are able to compare our data to previously determined hydration rates of obsidians (Riciputi et al., 2002; Eerkens et al., 2008). In addition, we focus on six tephra units ranging from basalt to rhyolite that have different porosities, which we measure, to constrain the influence of vesicularity and composition on the secondary hydration process. Using this information, we then create simplified hydration models utilizing our water concentration and age data to estimate the diffusivities for secondary hydration of felsic and mafic glass.

2. METHODS

2.1. Samples

We use basaltic andesite scoria collected by us from Klyuchevskoy volcano in Kamchatka, Russia, with ages ranging from 0.05 to 7.3 ka (Auer et al., 2009). This volcanic scoria was used specifically due to the similar basaltic andesite composition of all samples collected from the same trench across an approximately 7000 year time span (Ponomareva et al., 2007, 2013; Auer et al., 2009). Other mafic samples from Kamchatka include: the 3.5 and 7.2 ka eruptions of Avachinsky volcano, the 7.5 ka eruption of Kizimen, the 0.05, 1.0, 1.5, and 2.8 ka eruptions of Shiveluch volcano, and the voluminous pyroclastic products from the 7.6 ka caldera-forming eruption of Kurile Lake (Braitseva et al., 1997; Ponomareva et al., 2004; Kyle et al., 2011). We also analyzed mafic samples from Tanzania that include the 2.0 and 4.0 ka eruptions of Rungwe (Fontijn et al., 2010) (Tables 1 and 2; Fig. 1).

Felsic tephra samples were collected from Kamchatka, Chile, and the United States (Tables 1 and 2; Fig. 1). The Kamchatka units include: the 7.9 ka eruption of Karymsky volcano, the 1.8 and 6.4 ka eruptions of Ksudach volcano, the 7.6 ka eruption of Kurile Lake, the 0.3 and 3.5 ka eruptions of Opala volcano, the 7.0 ka eruption of Khangar volcano, and the 1.5 and 4.6 ka Optr eruptions (Braitseva et al., 1997). Chilean units are from the: 10 ka Llaima, 3.0 ka Sollipulli, and 4.5 ka Puyehue-Cordon Caulle eruptions (Fontijn et al., 2014). We also collected multiple samples throughout Oregon from the 7.7 ka Mt. Mazama eruption that formed Crater Lake.

All samples analyzed in this study are $\leqslant$10,000 years old. Based on their relatively young, post-glacial Holocene ages, we assume that they are hydrated with meteoric water that has approximately similar δD to current precipitation. Therefore, all samples should be young enough that the δD (‰) of the meteoric water hydrating them should not be significantly changing on a millennial timescale (e.g. Henderson et al., 2010, which suggests 15–20‰ shifts in δD over the last 10,000 years).

2.2. Hydrogen isotope and total water analyses of tephra and ash

All volcanic glass samples from this study were analyzed for both δD and H_2O_t on the TCEA (Thermal Conversion Elemental Analyzer) continuous flow and sampling system at the University of Oregon stable isotope laboratory (e.g. Bindeman et al., 2012). Prior to analysis, tephra samples were lightly crushed, placed in a water-filled beaker, and sonicated for ~60 min to remove any clays that, if present, may be attached to the glass. The samples were then dried and individual glass shards smaller than ~0.5 mm were picked under microscope to ensure that the glass was pristine. We first experimented with pretreating samples with 8% HF twice for 30 seconds (Cerling et al., 1985; Sarna-Wojcicki and Davis, 1991; Cassel et al., 2012), but found that such a procedure yields greater scatter (Fig. A1) and abandoned this approach because our samples are fresh and do not contain any secondary 'gel' layer as for the above-mentioned studies. Our results, which are similar to those from Dettinger and Quade (2015) that show glass samples pretreated with HF having variable δD effects in glass that are not well understood, we chose not to pretreat any samples in 8% HF. Following sample preparation, 2–12 mg of glass (depending on the expected water content, where the lowest water content samples need the largest mass of glass) were picked using a binocular microscope and packaged in silver foil. Ash samples were sieved to keep the 50–250 μm size fraction, as demonstrated by experimentation with glass standards to yield the best reproducibility (Bindeman et al., 2012). Some ash samples contain too many small phenocrysts (microphenocrysts or microlites) to be completely separated from the glass. For these samples, a modal percent of minerals was approximated, and the wt.% H_2O_t was corrected following the analysis (Table 3). These small phenocrysts were all determined to be anhydrous, so a correction was only needed for the wt.% H_2O_t and not for the δD value. Prior to analysis, all samples were heated in a vacuum-sealed oven overnight at 130 °C to remove any adsorbed waters on the outer surface of the glass (e.g. Nolan and Bindeman, 2013). Samples were then immediately loaded into a TCEA autosampler (typically within 10–15 min), where they were purged with He carrier gas.

The first part of this study included standardization using three mica reference standards during each set of analyses (NBS30 biotite, $\delta D = -65.7$‰, and two other in house standards calibrated relative to NBS30 in three other labs: BUD Butte (MT) quartz monzonite biotite, $\delta D = -161.8$‰, and RUH2 muscovite, $\delta D = -98.2$‰), which nearly span the range of our unknowns. Following each set of analyses, a three point calibration using the offsets between the measured and nominal δD values

Table 1
Location, age, and local precipitation δD (‰, VSMOW) of glass samples.

Sample Name	Volcano	Region	Age (ka)	Location N	Location E	Elevation (m)	Current local δD (‰) of precipitation
99163/9	Avachinsky	Kamchatka	3.50	53.32	158.91	826	−124
99201/1	Avachinsky	Kamchatka	7.15	53.25	159.04	369	−117
VF-74-200	Volcán de Fuego	Guatemala	0.04	14.50[a]	−90.90[a]	2579	−69
VF-74-45	Volcán de Fuego	Guatemala	0.04	14.50[a]	−90.90[a]	2579	−69
808 KAR 4	Karymsky	Kamchatka	7.90	54.03	159.18	294	−120
Margomulyo-1p	Kelud	Indonesia	0.00	−7.93	112.24	617	−42
Campling-4p	Kelud	Indonesia	0.00	−7.97	112.18	329	−38
98032/4	Khangar	Kamchatka	7.00	54.95	157.50	935	−134
80013/4	Kizimen	Kamchatka	7.50	54.88	160.37	376	−124
KLV5-1	Klyuchevksoy	Kamchatka	0.05	56.14	160.80	922	−136
KLV5-10	Klyuchevksoy	Kamchatka	3.10	56.14	160.80	922	−136
KLV5-11	Klyuchevksoy	Kamchatka	3.20	56.14	160.80	922	−136
KLV5-12	Klyuchevksoy	Kamchatka	3.40	56.14	160.80	922	−136
KLV5-13	Klyuchevksoy	Kamchatka	3.60	56.14	160.80	922	−136
KLV5-15	Klyuchevksoy	Kamchatka	4.70	56.14	160.80	922	−136
KLV5-18a	Klyuchevksoy	Kamchatka	5.70	56.14	160.80	922	−136
KLV5-22	Klyuchevksoy	Kamchatka	7.30	56.14	160.80	922	−136
KLV5-3	Klyuchevksoy	Kamchatka	1.00	56.14	160.80	922	−136
KLV5-5	Klyuchevksoy	Kamchatka	1.60	56.14	160.80	922	−136
KLV5-6	Klyuchevksoy	Kamchatka	2.30	56.14	160.80	922	−136
KLV5-7	Klyuchevksoy	Kamchatka	2.60	56.14	160.80	922	−136
KLV5-8	Klyuchevksoy	Kamchatka	2.70	56.14	160.80	922	−136
KLV5-9	Klyuchevksoy	Kamchatka	2.80	56.14	160.80	922	−136
8880/5	Ksudach	Kamchatka	1.80	51.87[a]	157.53[a]	318	−112
8889/2	Ksudach	Kamchatka	6.40	51.87[a]	157.53[a]	318	−112
97KAM-03a	Kurile Lake	Kamchatka	7.60	51.50	156.53	19.2	−107
97KAM11	Kurile Lake	Kamchatka	7.60	51.50	156.53	19.2	−107
97KAM29AL	Kurile Lake	Kamchatka	7.60	51.38	157.27	73.2	−107
97KAM29DL	Kurile Lake	Kamchatka	7.60	51.38	157.27	73.2	−107
97KAM29HW	Kurile Lake	Kamchatka	7.60	51.38	157.27	73.2	−107
97KAM32D1	Kurile Lake	Kamchatka	7.60	51.36	157.27	60.7	−107
97KAM-21CG	Kurile Lake	Kamchatka	7.60	51.50	157.02	364	−112
97KAM-29AB	Kurile Lake	Kamchatka	7.60	51.38	157.27	73.2	−107
97KAM29DB	Kurile Lake	Kamchatka	7.60	51.38	157.27	73.2	−107
CLD205 J	Llaima	Chile	10.00	−38.76	−71.62	782	−62
2013MM-1	Mt. Mazama	Oregon	7.70	43.92	−121.34	1366	−106
2013MM-10	Mt. Mazama	Oregon	7.70	43.54	−121.95	1466	−107
2013MM-11	Mt. Mazama	Oregon	7.70	43.48	−121.90	1419	−106
2013MM-12	Mt. Mazama	Oregon	7.70	43.45	−121.87	1449	−106
2013MM-13	Mt. Mazama	Oregon	7.70	43.38	−121.80	1434	−106
2013MM-14	Mt. Mazama	Oregon	7.70	43.18	−121.79	1447	−106
2013MM-15	Mt. Mazama	Oregon	7.70	43.09	−122.21	1650	−108
2013MM-16	Mt. Mazama	Oregon	7.70	43.05	−122.35	1193	−102
2013MM-18	Mt. Mazama	Oregon	7.70	43.14	−122.01	1887	−112
2013MM-2	Mt. Mazama	Oregon	7.70	43.41	−121.22	1410	−106
2013MM-3	Mt. Mazama	Oregon	7.70	43.43	−121.28	1433	−106
2013MM-4	Mt. Mazama	Oregon	7.70	43.46	−121.39	1436	−106
2013MM-5	Mt. Mazama	Oregon	7.70	43.52	−121.46	1327	−105
2013MM-6	Mt. Mazama	Oregon	7.70	43.60	−121.50	1301	−105
2013MM-7	Mt. Mazama	Oregon	7.70	43.59	−121.57	1310	−105
2013MM-8	Mt. Mazama	Oregon	7.70	43.47	−121.70	1362	−105
2013MM-9	Mt. Mazama	Oregon	7.70	43.56	−121.96	1479	−107
2014MM-1	Mt. Mazama	Oregon	7.70	44.10	−119.99	1426	−108
Mazama-WMC	Mt. Mazama	Oregon	7.70	44.43	−120.60	1201	−105
42-Cordova	Mt. Spurr	Alaska	0.02	61.3[a]	−152.30[a]	2795	−160
57-Ashton	Mt. Spurr	Alaska	0.02	61.3[a]	−152.30[a]	2795	−160
98-10	Opala	Kamchatka	0.30	52.55[a]	157.39[a]	823	−122
98-33/2	Opala	Kamchatka	3.50	52.43	157.33	172	−112
98KAM2.3	Optr	Kamchatka	4.60	52.63	157.48	385	−116
98KAM2.4	Optr	Kamchatka	1.50	52.63	157.48	385	−116
CLD155A	Puyehue-Cordon Caulle	Chile	4.50	−40.25	−72.22	178	−58
KF149B	Rungwe	Tanzania	4.00	−9.05	33.63	2035	−38
KF155D	Rungwe	Tanzania	2.00	−9.08	33.57	1856	−35
96025/4	Shiveluch	Kamchatka	1.00	56.57	161.51	372	−129
97044/1	Shiveluch	Kamchatka	0.05	56.65	161.46	1028	−139
97049/2	Shiveluch	Kamchatka	1.45	56.65	161.46	1028	−139
97051/2	Shiveluch	Kamchatka	2.80	56.65	161.46	1028	−139
CLD064B	Sollipulli	Chile	3.00	−39.07	−72.52	979	−66

[a] Approximate sample location.

Table 2
δD (‰, VSMOW) (pre and post magmatic correction) and wt.% H_2O_t of water extracted from glass for each sample.

Sample Name	Volcano	Age (ka)	Composition	Number analyses	δD (‰)	s.d.	H_2O_t (wt.%)	s.d.	δD (‰) magmatic corrected
99163/9	Avachinsky	3.50	Basaltic andesite	3	−112	2.2	0.25	0.02	NA
99201/1	Avachinsky	7.15	Andesite	3	−95	3.5	1.42	0.26	−113
VF-74-200	Fuego	0.04	Basalt	3	−86	3.7	0.22	0.01	NA
VF-74-45	Fuego	0.04	Basalt	3	−86	6.4	0.07	0.01	NA
808 KAR 4	Karymsky	7.90	Dacite	3	−141	1.6	3.39	0.07	−149
Margomulyo-1p	Kelud	0.00	Basaltic andesite	2	−69	7.1	0.05	0.01	NA
Campling-4p	Kelud	0.00	Basaltic andesite	3	−73	1.6	0.05	0.01	NA
98032/4	Khangar	7.00	Dacite	3	−138	0.7	2.19	0.05	−150
80013/4	Kizimen	7.50	Andesite	2	−129	0.2	3.16	0.21	−137
KLV5-1	Klyuchevksoy	0.05	Basaltic andesite	4	−88	4.5	0.28	0.02	NA
KLV5-10	Klyuchevksoy	3.10	Basaltic andesite	4	−95	2.8	0.59	0.01	−146
KLV5-11	Klyuchevksoy	3.20	Basaltic andesite	6	−109	3.7	0.43	0.07	−179
KLV5-12	Klyuchevksoy	3.40	Basaltic andesite	3	−100	4.7	0.42	0.05	−173
KLV5-13	Klyuchevksoy	3.60	Basaltic andesite	3	−105	0.0	0.25	0.00	NA
KLV5-15	Klyuchevksoy	4.70	Basalt	4	−93	5.6	1.03	0.02	−123
KLV5-18a	Klyuchevksoy	5.70	Basaltic andesite	2	−92	1.9	0.45	0.02	−160
KLV5-22	Klyuchevksoy	7.30	Basaltic andesite	4	−93	2.2	0.64	0.03	−140
KLV5-3	Klyuchevksoy	1.00	Basaltic andesite	4	−85	6.8	0.39	0.04	NA
KLV5-5	Klyuchevksoy	1.60	Basaltic andesite	6	−87	1.4	0.40	0.03	−162
KLV5-6	Klyuchevksoy	2.30	Basaltic andesite	3	−95	1.7	0.29	0.01	NA
KLV5-7	Klyuchevksoy	2.60	Basaltic andesite	6	−103	3.0	0.45	0.06	−170
KLV5-8	Klyuchevksoy	2.70	Basaltic andesite	4	−91	0.0	0.30	0.00	NA
KLV5-9	Klyuchevksoy	2.80	Basaltic andesite	2	−94	3.1	0.34	0.02	NA
8880/5	Ksudach	1.80	Dacite	1	−122	0.0	3.35	0.00	−129
8889/2	Ksudach	6.40	Dacite	3	−116	2.0	1.66	0.13	−132
97KAM-03a	Kurile Lake	7.60	Rhyolite	4	−107	2.7	3.11	0.12	−116
97KAM11	Kurile Lake	7.60	Rhyolite	3	−110	3.3	2.51	0.09	−120
97KAM29AL	Kurile Lake	7.60	Rhyolite	3	−115	4.2	2.31	0.14	−126
97KAM29DL	Kurile Lake	7.60	Rhyolite	3	−120	3.4	2.29	0.15	−131
97KAM29HW	Kurile Lake	7.60	Dacite	3	−128	5.6	2.66	0.09	−138
97KAM32D1	Kurile Lake	7.60	Dacite	3	−123	0.9	3.08	0.10	−131
97KAM-21CG	Kurile Lake	7.60	Andesite	2	−112	3.1	1.10	0.10	−138
97KAM-29AB	Kurile Lake	7.60	Basaltic andesite	3	−111	1.1	0.27	0.06	NA
97KAM29DB	Kurile Lake	7.60	Basalt	3	−93	2.6	0.86	0.11	−124
CLD205J	Llaima	10.00	Dacite	3	−99	5.5	2.51	0.06	−109
2013MM-1	Mt. Mazama	7.70	Rhyolite	3	−140	6.7	3.07	0.17	−149
2013MM-10	Mt. Mazama	7.70	Rhyolite	3	−110	2.2	4.31	0.01	−117
2013MM-11	Mt. Mazama	7.70	Rhyolite	3	−124	8.7	2.74	0.26	−134
2013MM-12	Mt. Mazama	7.70	Rhyolite	3	−124	6.2	3.54	0.02	−132
2013MM-13	Mt. Mazama	7.70	Rhyolite	3	−129	0.0	2.85	0.00	−139
2013MM-14	Mt. Mazama	7.70	Rhyolite	3	−139	6.3	2.98	0.09	−148
2013MM-15	Mt. Mazama	7.70	Rhyolite	6	−130	1.7	4.25	0.37	−136
2013MM-16	Mt. Mazama	7.70	Rhyolite	3	−111	4.5	2.02	0.11	−124
2013MM-18	Mt. Mazama	7.70	Rhyolite	3	−111	2.0	2.10	0.74	−124
2013MM-2	Mt. Mazama	7.70	Rhyolite	3	−135	0.0	3.54	0.00	−142
2013MM-3	Mt. Mazama	7.70	Rhyolite	3	−147	6.8	2.70	0.18	−156
2013MM-4	Mt. Mazama	7.70	Rhyolite	3	−147	6.0	2.73	0.15	−156
2013MM-5	Mt. Mazama	7.70	Rhyolite	3	−144	5.9	2.77	0.27	−154
2013MM-6	Mt. Mazama	7.70	Rhyolite	3	−139	9.2	3.20	0.15	−147
2013MM-7	Mt. Mazama	7.70	Rhyolite	3	−129	1.1	3.30	0.21	−137
2013MM-8	Mt. Mazama	7.70	Rhyolite	3	−123	0.0	3.34	0.00	−131
2013MM-9	Mt. Mazama	7.70	Rhyolite	3	−116	6.4	3.68	0.05	−124
2014MM-1	Mt. Mazama	7.70	Rhyolite	3	−110	3.4	4.72	0.18	−116
Mazama-WMC	Mt. Mazama	7.70	Rhyolite	2	−138	0.0	2.59	0.00	−148
42-Cordova	Mt. Spurr	0.02	Andesite	4	−89	3.6	0.57	0.03	NA
57-Ashton	Mt. Spurr	0.02	Andesite	4	−93	3.5	0.58	0.05	NA
98-10	Opala	0.30	Rhyolite	3	−100	7.7	0.53	0.35	−151
98-33/2	Opala	3.50	Dacite	3	−106	3.1	1.81	0.18	−120
98KAM2.3	Optr	4.60	Dacite	3	−123	1.0	2.14	0.21	−136
98KAM2.4	Optr	1.50	Rhyolite	3	−103	3.4	2.73	0.07	−113
CLD155A	Puyehue-Cordon Caulle	4.50	Dacite	6	−95	3.4	3.22	0.30	−103
KF149B	Rungwe	4.00	Andesite	6	−92	5.8	2.91	0.91	−101
KF155D	Rungwe	2.00	Andesite	6	−73	2.4	2.39	0.22	-84
96025/4	Shiveluch	1.00	Andesite	3	−116	3.6	1.06	0.14	−141
97044/1	Shiveluch	0.05	Andesite	3	−82	2.2	0.61	0.03	NA
97049/2	Shiveluch	1.45	Basaltic andesite	2	−127	2.0	0.94	0.08	−155
97051/2	Shiveluch	2.80	Andesite	3	−112	6.9	1.15	0.19	−135
CLD064B	Sollipulli	3.00	Dacite	3	−97	0.9	2.05	0.22	−110

Table 3
Relative vesicularity and percent microlites of glass samples.

Sample Name	Volcano	Age (ka)	Relative vesicularity (1–10)	Microlites (%)
99163/9	Avachinsky	3.50	2	1
99201/1	Avachinsky	7.15	3	5
VF-74-200	Fuego	0.04	10	15
VF-74-45	Fuego	0.04	10	15
808 KAR 4	Karymsky	7.90	8	0
Margomulyo-1p	Kelud	0.00	5	2
Campling-4p	Kelud	0.00	5	2
98032/4	Khangar	7.00	7	3
80013/4	Kizimen	7.50	6	0
KLV5-1	Klyuchevksoy	0.05	3	30
KLV5-10	Klyuchevksoy	3.10	2	35
KLV5-11	Klyuchevksoy	3.20	3	30
KLV5-12	Klyuchevksoy	3.40	1	40
KLV5-13	Klyuchevksoy	3.60	2	20
KLV5-15	Klyuchevksoy	4.70	4	35
KLV5-18a	Klyuchevksoy	5.70	4	30
KLV5-22	Klyuchevksoy	7.30	2	50
KLV5-3	Klyuchevksoy	1.00	2	40
KLV5-5	Klyuchevksoy	1.60	2	20
KLV5-6	Klyuchevksoy	2.30	4	10
KLV5-7	Klyuchevksoy	2.60	4	20
KLV5-8	Klyuchevksoy	2.70	4	30
KLV5-9	Klyuchevksoy	2.80	4	20
8880/5	Ksudach	1.80	8	0
8889/2	Ksudach	6.40	8	0
97KAM-03a	Kurile Lake	7.60	9	0
97KAM11	Kurile Lake	7.60	5	1
97KAM29AL	Kurile Lake	7.60	5	2
97KAM29DL	Kurile Lake	7.60	9	0
97KAM29HW	Kurile Lake	7.60	9	0
97KAM32D1	Kurile Lake	7.60	6	2
97KAM-21CG	Kurile Lake	7.60	9	1
97KAM-29AB	Kurile Lake	7.60	8	2
97KAM29DB	Kurile Lake	7.60	8	2
CLD205 J	Llaima	10.00	8	0
2013MM-1	Mt. Mazama	7.70	7	0
2013MM-10	Mt. Mazama	7.70	7	0
2013MM-11	Mt. Mazama	7.70	7	0
2013MM-12	Mt. Mazama	7.70	7	0
2013MM-13	Mt. Mazama	7.70	7	0
2013MM-14	Mt. Mazama	7.70	7	0
2013MM-15	Mt. Mazama	7.70	7	0
2013MM-16	Mt. Mazama	7.70	7	0
2013MM-18	Mt. Mazama	7.70	7	0
2013MM-2	Mt. Mazama	7.70	7	0
2013MM-3	Mt. Mazama	7.70	7	0
2013MM-4	Mt. Mazama	7.70	7	0
2013MM-5	Mt. Mazama	7.70	7	0
2013MM-6	Mt. Mazama	7.70	7	0
2013MM-7	Mt. Mazama	7.70	7	0
2013MM-8	Mt. Mazama	7.70	7	0
2013MM-9	Mt. Mazama	7.70	7	0
2014MM-1	Mt. Mazama	7.70	7	0
Mazama-WMC	Mt. Mazama	7.70	8	0
42-Cordova	Mt. Spurr	0.02	10	30
57-Ashton	Mt. Spurr	0.02	10	30
98-10	Opala	0.30	8	0
98-33/2	Opala	3.50	7	0
98KAM2.3	Optr	4.60	7	0
98KAM2.4	Optr	1.50	8	0
CLD155A	Puyehue-Cordon Caulle	4.50	7	0
KF149B	Rungwe	4.00	8	0
KF155D	Rungwe	2.00	7	0
96025/4	Shiveluch	1.00	5	5
97044/1	Shiveluch	0.05	4	5
97049/2	Shiveluch	1.45	4	5
97051/2	Shiveluch	2.80	5	5
CLD064B	Sollipulli	3.00	7	0

Table 4
Textural data for BSE imaged tephra from Kurile Lake and Klyuchevskoy volcanoes in Kamchatka, Russia.

Unit	Volcano	Age (ka)	Composition	Region of clast	Area (mm^2)	Total Perimeter (mm)	Number	Number per Unit Area (mm^{-2})	Average Bubble Wall Thickness (mm)
KLV5-1	Klyuchevskoy	0.05	Basaltic andesite	Total	34.0	92.8	1		0.103
				Minerals	0.71	8.08	7		
				Vesicles	15.6	450	899	27	
				Glass	17.7				
KLV5-8	Klyuchevskoy	2.7	Basaltic andesite	Total	23.7	63.4	1		0.075
				Minerals	0.72	7.29	5		
				Vesicles	12.1	248	650	28	
				Glass	10.9				
KLV5-22	Klyuchevskoy	7.3	Basaltic andesite	Total	24.6	52.6	1		0.051
				Minerals	1.23	12.4	13		
				Vesicles	13.8	442	1695	72	
				Glass	9.62				
97KAM29AL	Kurile Lake	7.6	Rhyolite	Total	36.8	109	1		0.017
				Minerals	0.16	3.80	6		
				Vesicles	13.1	2078	26983	736	
				Glass	23.6				
97KAM29DB	Kurile Lake	7.6	Basalt	Total	96.7	159	1		0.058
				Minerals	32.7	224	129		
				Vesicles	32.9	1447	4953	77	
				Glass	31.2				
97KAM21CG	Kurile Lake	7.6	Andesite	Total	31.0	59.4	1		0.030
				Minerals	4.80	55.0	35		
				Vesicles	9.08	554	4215	161	
				Glass	17.2				

for the mica standards was performed to correct for day-to-day analytical variations in δD values. These same analyses were also used to determine the total water content in the glass. NBS30, with a known wt.% H_2O_t of 3.5 was used as a standard for water concentration corrections.

In order to present our results relative to VSMOW, we ran glass samples in the latter part of this study against water (VSMOW, W62001, and GISP) sealed in silver cups (Qi et al., 2010). This extra step was necessary due to a recent study by Qi et al. (2014), which demonstrated that the NBS30 nominal δD value is 15–21‰ heavier than previously proposed. We therefore ran all of our mica standards (NBS30, BUD, and RUH2) directly against these waters sealed in silver cups, which have δD values spanning the relevant δD range of our solids. This was done to calibrate the δD of water extracted from the micas for our lab specifically relative to a water-based VSMOW scale. For further information on the correction of the NBS30 standard, see Qi et al. (2014), which is what we base our lab specific corrections on. Through seven different analytical sessions of calibration between our mica standards and the three water standards, we obtain a conversion equation of: $\delta D_{micacorrected} = 0.9888\delta D_{initial} + 15.385$, with an R^2 of 0.99179. We use this conversion equation to correct all of our mica data, which provided a correction of +16–17‰ to our old mica-based normalization, depending on the δD value. The data below are all reported with respect to the water standards we utilize in this study (VSMOW, GISP, and W62001).

2.3. SEM imaging of volcanic tephra to determine surface to volume ratios and bubble wall thicknesses

Six tephra units shown in Table 4 with known water content and δD were imaged with Back-Scattered Electrons (BSE). These tephra were chosen to provide a range of vesicularity and bubble wall thickness for mafic units of various ages from the same volcano (Klyuchevskoy), as well as for a range in compositions from the same compositionally diverse eruption (Kurile Lake). These six tephra were photographed under high magnification using a FEI Quanta 200 SEM microscope at 20 keV, allowing submicron resolution (Fig. 4). The photographs were converted to black and white in Adobe Photoshop and checked to make sure all black regions were vesicles (Fig. 5). If they were not, they were changed to white, and vice versa. A separate image was then created so that the entire tephra clast, including vesicles, was all one color. This allowed for the entire area of the tephra clast and vesicles to be determined. Another image was created with just the minerals shown in black, so these areas could be removed from any subsequent calculations. All images were imported into the image-processing program NIH ImageJ, which was used to determine the number of vesicles, the area of each vesicle, the perimeter of each vesicle, the total area of the tephra clast including the vesicles and the glass, and the area of the minerals (Fig. 6). The perimeter of each vesicle was assumed to create a circle, and the radius of each vesicle was calculated from: $R = \frac{P}{2\pi}$, where R is the radius of the assumed circle in mm and P is the perimeter in mm.

Following Giachetti and Gonnermann (2013), we assumed that the vesicles are distributed evenly across the tephra clast (i.e., we use the hexagonal close-packing assumption of Princen (1979) and Proussevitch et al. (1993)) and estimated the average bubble wall thickness for each tephra clast using the equation: $S = \frac{R}{\phi^{\frac{1}{3}}}$, where S is the average thickness of the bubble wall in mm, ϕ is the vesicularity, and R is again the radius in mm. As a check, these values were compared to the SEM tephra clast images (Figs. 4–6) to ensure that they are indeed reasonable.

3. RESULTS

We report data from Holocene ash and tephra and provide a range of water concentrations and D/H from 0 to 10 ka volcanic glass of both mafic and felsic composition to better understand hydration rates and corresponding D/H trends with secondary hydration.

3.1. Water concentration and hydrogen isotopes in felsic and mafic ashes and scoria

3.1.1. Recently deposited felsic ash samples

The recently deposited ash from the 1992 eruption of Mt. Spurr (42-Cordova and 57-Ashton), the 1974 eruption of Volcán de Fuego (VF-74-45 and VF-74-200), and the 2014 eruption of Kelud (Margomulyo-1p and Campling-4p) are used to gain a better understanding of the quantity of residual undegassed magmatic water dissolved in the glass that volcanic ash is deposited with, and the δD of these associated dissolved waters. These glasses were all collected either during or recently following eruption, so they are assumed to contain only magmatic water, and provide a constraint on the H_2O_t and D/H of primary magmatic water. These data plot within the magmatic degassing trend in Fig. 2. The H_2O_t of these samples ranges from 0.1 to 0.6 wt.% H_2O_t and the δD ranges from −69 to −93‰.

3.1.2. Mass balance relations

Results above indicate that unaltered volcanic ash can contain as much as ~0.6 wt.% magmatic water. Although these quantities vary from one tephra layer to the next (0.1–0.6 wt.%), the average water content is 0.3 wt.%. With these data, we can account for the influence of primary magmatic water using mass balance equations:

$$H_2O_t = H_2O_{t,met} + H_2O_{t,mag} \quad (2)$$

$$\delta D_t \approx F_{met}(\delta D_{met} - \Delta_{water-glass}) + (1 - F_{met})(\delta D_{mag}) \quad (3)$$

where F is the fraction by weight of water in glass that is meteoric, t,met designates the total secondary meteoric water (hydroxyl and molecular), t,mag designates the total primary magmatic water, and $\Delta_{water\text{-}glass}$ is equal to δ_{water}-δ_{glass}. These mass balance equations describe the variations between the quantity of residual magmatic water left in the glass following deposition, and the relative quantity of secondary hydration. This relation is illustrated in Fig. 7, which shows the effect that residual magmatic water can have on the total δD values during analysis of the glass, indicating a need for a correction for primary magmatic water during δD analyses of hydrated volcanic glass, which will be discussed further below.

3.1.3. Hydration of mafic glass

Water concentrations versus the ages of volcanic scoria from Klyuchevskoy volcano show that there is a general trend of slightly increasing wt.% H_2O_t and decreasing δD (‰) with age (Figs. 8, A2). The youngest samples, with ages younger than ~0.2 ka, have ~0.4 wt.% H_2O_t on average. The older samples, ages 4.7–7.3 ka, have slightly higher water concentrations (~0.4 to 1.0 wt.%). Given the low δD of precipitation in Kamchatka (−136‰; interpolated value from Bowen and Revenaugh, 2003; Bowen, 2015), the decrease in δD with increasing age and water content is an isotopic indication of minor secondary hydration.

In addition to the stratigraphic sequence of the Klyuchevskoy scoria, we analyzed mafic tephra (⩽63 wt.% SiO_2) with a range in age and water concentrations from around Kamchatka and Tanzania to obtain further hydration and δD trends of mafic tephra worldwide (Tables 1 and 2; Fig. 1). Although the majority of these tephra were more hydrated than the Klyuchevskoy scoria, their water contents generally do not exceed 2.0 wt.% H_2O_t, even for the tephra that are up to 7.6 ka. Only three glass samples have higher water concentrations: the 2.0 and 4.0 ka eruption of Rungwe and the 7.5 ka eruption of Kizimen. The trend of decreasing δD (‰) with increasing wt.% of added secondary H_2O_t is most clear up to ~1.5 wt.% H_2O_t, after which the δD values become more scattered (−129 to −73‰). This is likely due to the differing δD of local meteoric water, as the scatter is mostly due to the hydrated Tanzania samples from a lower latitude, where we see δD of precipitation that is near 100‰ heavier than at the higher latitude regions. (Figs. 1 and 2).

3.1.4. Hydration of felsic glass

Felsic tephra from varying climates all show a clear trend of increasing water and decreasing δD within the first 1500 years, when compared to the recently deposited tephra (Fig. 8). Water concentrations of the felsic glasses have ~0.5 wt.% H_2O_t at 300 years and have up to ~3.0 wt.% H_2O_t after 2700 years (Fig. 8). After ~2700 years, the water content generally stays near or above ~2.0 wt.% (±1.0 wt.% H_2O_t). This is in exception to three of the Mt. Mazama glass samples, which have higher H_2O_t between 4.0 and 5.0 wt.% (Figs. 2 and 8). Besides the recent ash, the youngest felsic glass analyzed here is the 300 year old Opala ash from Kamchatka with 0.5 wt.% H_2O_t, which is on the higher end of undegassed water concentrations of the recently deposited ash described above. At higher water contents (~2.0 to 3.5 wt.% H_2O_t), we observe a large range of δD values (~−147 to −95‰), which is again a reflection of the range in δD (‰) of precipitation around the world (Figs. 1 and 2).

3.2. Surface area as determined by SEM images of basalt versus rhyolite tephra

We examined clast textures and differences in surface areas of mafic versus felsic tephra on BSE images. The basalt-basaltic andesite units from Kurile Lake and

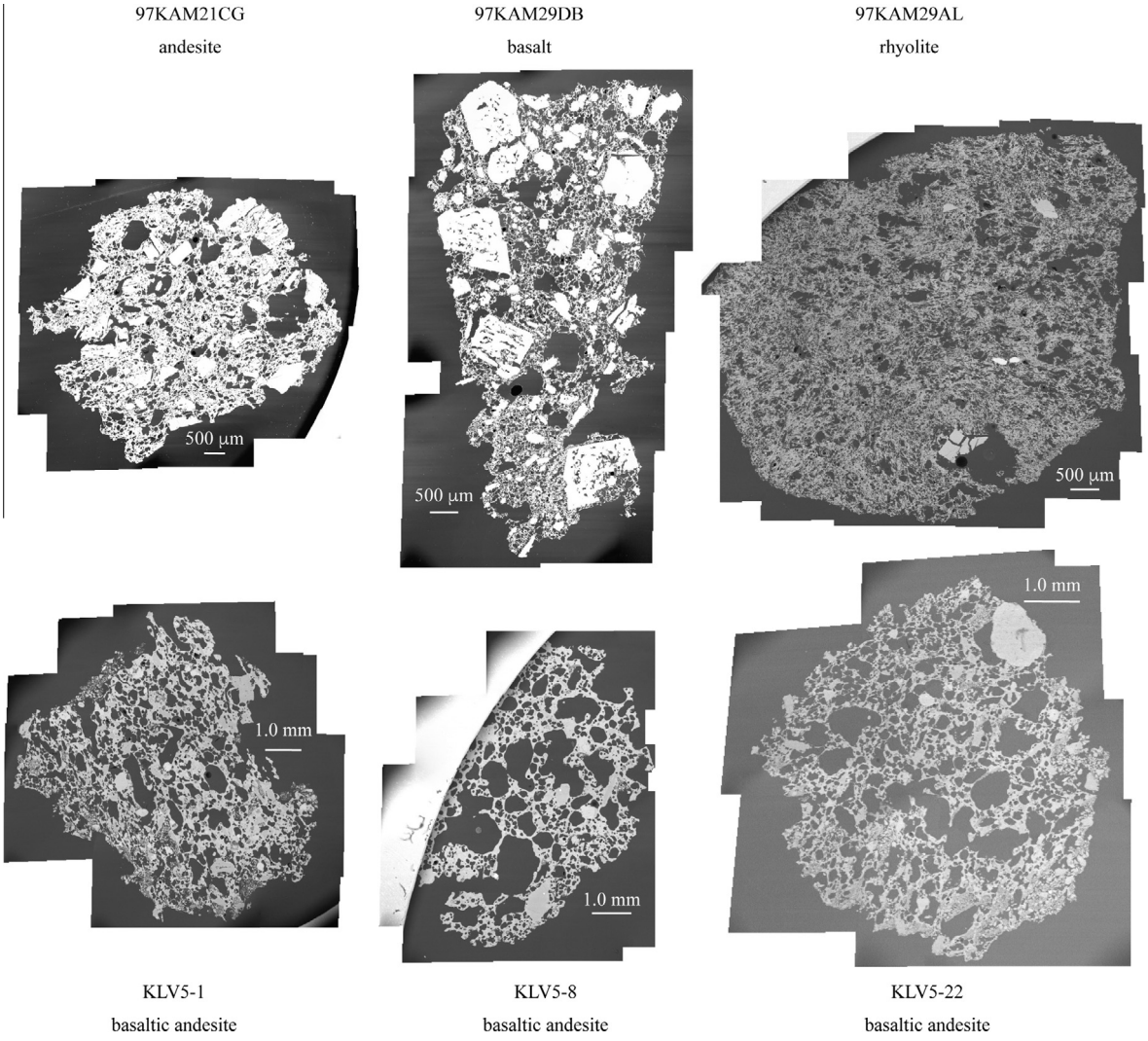

Fig. 4. BSE images of tephra used for basalt-andesite-rhyolite texture comparisons. Note the similarities of bubble number densities and bubble wall thicknesses in the Klyuchevskoy basaltic andesites (KLV5 units). The Klyuchevskoy units typically have fewer, yet larger, vesicles. In contrast, the basalt from the Kurile Lake eruption (97KAM29DB) generally has a larger number of smaller vesicles, which is likely due to the greater explosivity of the eruption. The rhyolite sample from the Kurile Lake eruption (97KAM29AL) has the most vesicles and the smallest bubble wall thicknesses in comparison to any of the basalts or andesites in this study (see Tables 3 and 4).

Klyuchevskoy have the lowest number of vesicles per unit area (25–77 mm^{-2}). Furthermore, the Klyuchevskoy basaltic andesites consistently have fewer vesicles per unit area (25–72 mm^{-2}) than all the Kurile Lake tephra clasts. The andesite from the Kurile Lake eruption has an intermediate value (161 mm^{-2}) and the rhyolite from the Kurile Lake eruption has the highest value (736 mm^{-2}) (Table 4). Similarly, the rhyolite tephra has the smallest average bubble wall thickness (0.02 mm), while the average bubble wall thickness for the basalt and basaltic andesites is 0.07 mm.

4. DISCUSSION

4.1. Mass balance analysis in distinguishing between magmatic and meteoric water

The importance of creating a magmatic water correction to better obtain the meteoric water δD signal is illustrated in Fig. 7. The wt.% residual H_2O_t and δD values are likely different at each volcano, so the magmatic correction needed for each volcano is likely different (and can be independently estimated using the youngest deposits), but we assume that similar looking tephra layers in the same section from a single volcano, such as Klyuchevskoy, can have identical residual H_2O_t and δD. To define a correction to remove the δD (‰) value of the primary magmatic water, we took an average δD (‰) and H_2O_t (wt.%) of the mafic tephra that have ages less than or equal to 1.0 ka and H_2O_t below 0.6 wt.%. The water concentration limit is based on the highest water concentration of the recently erupted ash (Mt. Spurr) and an age limit that is based on the low water concentration and high δD that we see for ash samples less than 1000 years old, indicating a lack of secondary hydration in these tephra. This provides an average δD and H_2O_t for nine degassed tephra of −83‰ (±7.7, 1 s.d.) and 0.32 wt.% (±0.2, 1 s.d.), respectively. Since we

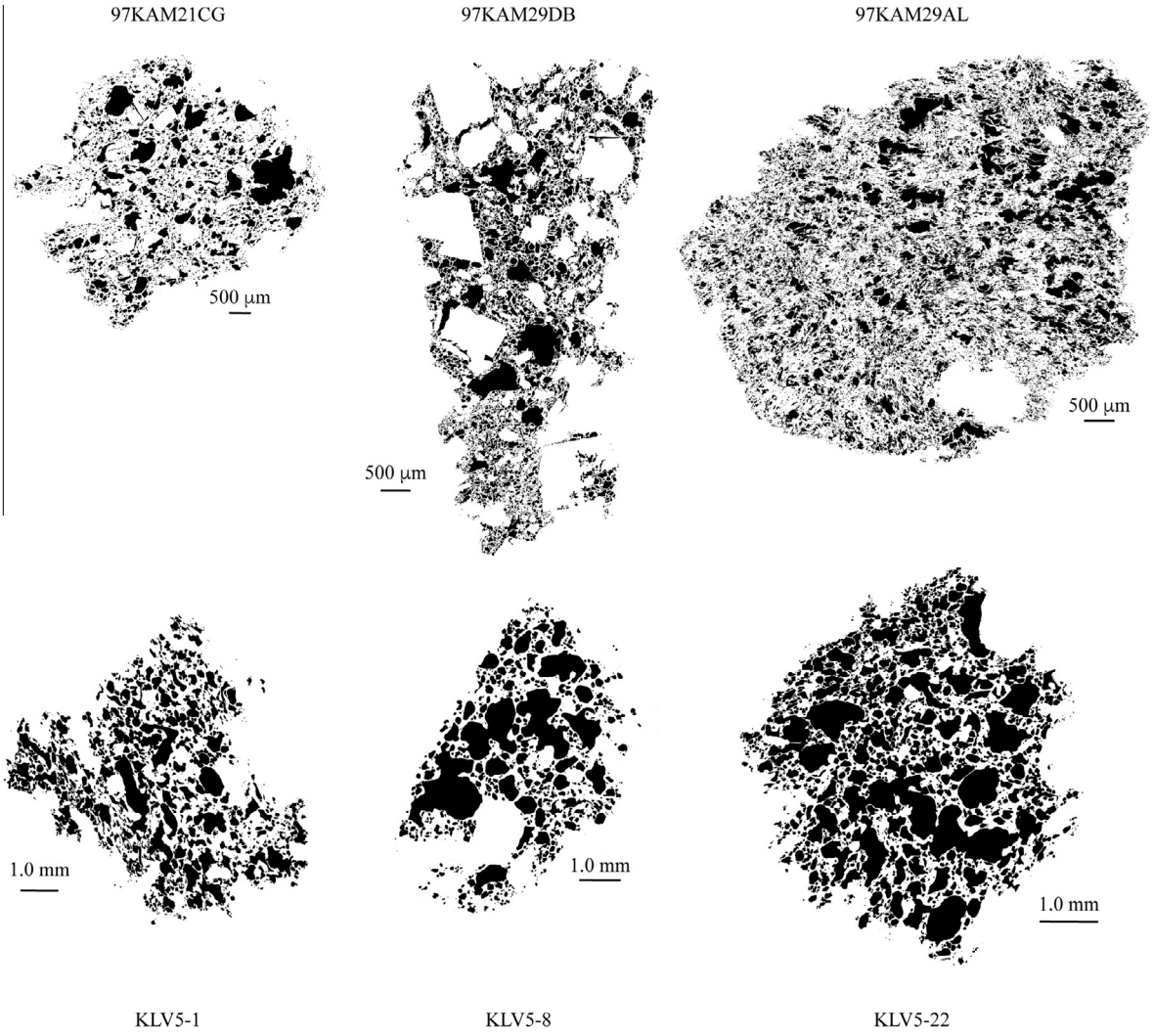

Fig. 5. Black and white vesicle images of tephra clasts that were created from the BSE images in Fig. 4. These images were used to determine the number, area, and perimeter of the vesicles for each tephra clast in ImageJ (see Fig. 6).

have a series of tephra from Klyuchevskoy volcano, we created a separate correction for the two Klyuchevskoy glasses of −86‰ δD (±2.2, 1 s.d.) and 0.35 wt.% H_2O_t (±0.1, 1 s.d.), which was determined by the two youngest Klyuchevskoy units (0.05 and 1.0 ka). Six basalt-basaltic andesite units are older than 1.0 ka, but have less total water than the correction factor (7.6 ka Kurile Lake, 3.5 ka Avachinsky, 2.3 ka Klyuchevskoy, 2.7 ka Klyuchevskoy, 2.8 ka Klyuchevskoy, 3.6 ka Klyuchevskoy). These units with low water concentrations are assumed to contain only primary magmatic water and were excluded from further analysis of secondary water determination when using the correction.

4.2. δD trends of secondary hydration as compared to local δD of precipitation

We compare the δD (‰) of the water in our glasses to local δD (‰) of meteoric waters, while taking into account the 0.9668 fractionation between meteoric water and water in volcanic glass, where glass is depleted in deuterium (Friedman et al., 1993a) (Fig. 9). Furthermore, we initially use the fractionation factor determined by Friedman et al. (1993a), which is intended for felsic glasses, on mafic glasses, and compare them to local meteoric waters to see if the fractionation factor is similar for mafic glasses, which is discussed further below. We also take into account our correction for total water and δD of primary magmatic water in this section, and do not discuss the isotopic characteristics of samples with water contents equal to or less than the magmatic water correction.

Prior to a magmatic water correction, our δD_{glass} values are typically heavier than their associated local meteoric waters (Figs. 9a, 10a). This can be explained if the water is mostly magmatic, as is illustrated in Figs. 2 and 7, since magmatic water remaining in the glass is commonly heavier in δD than the local meteoric water at higher latitudes (Fig. 1). This is particularly characteristic for many of the recently erupted ash and scoria samples with only magmatic water present in them that do not fall on the 1:1 line

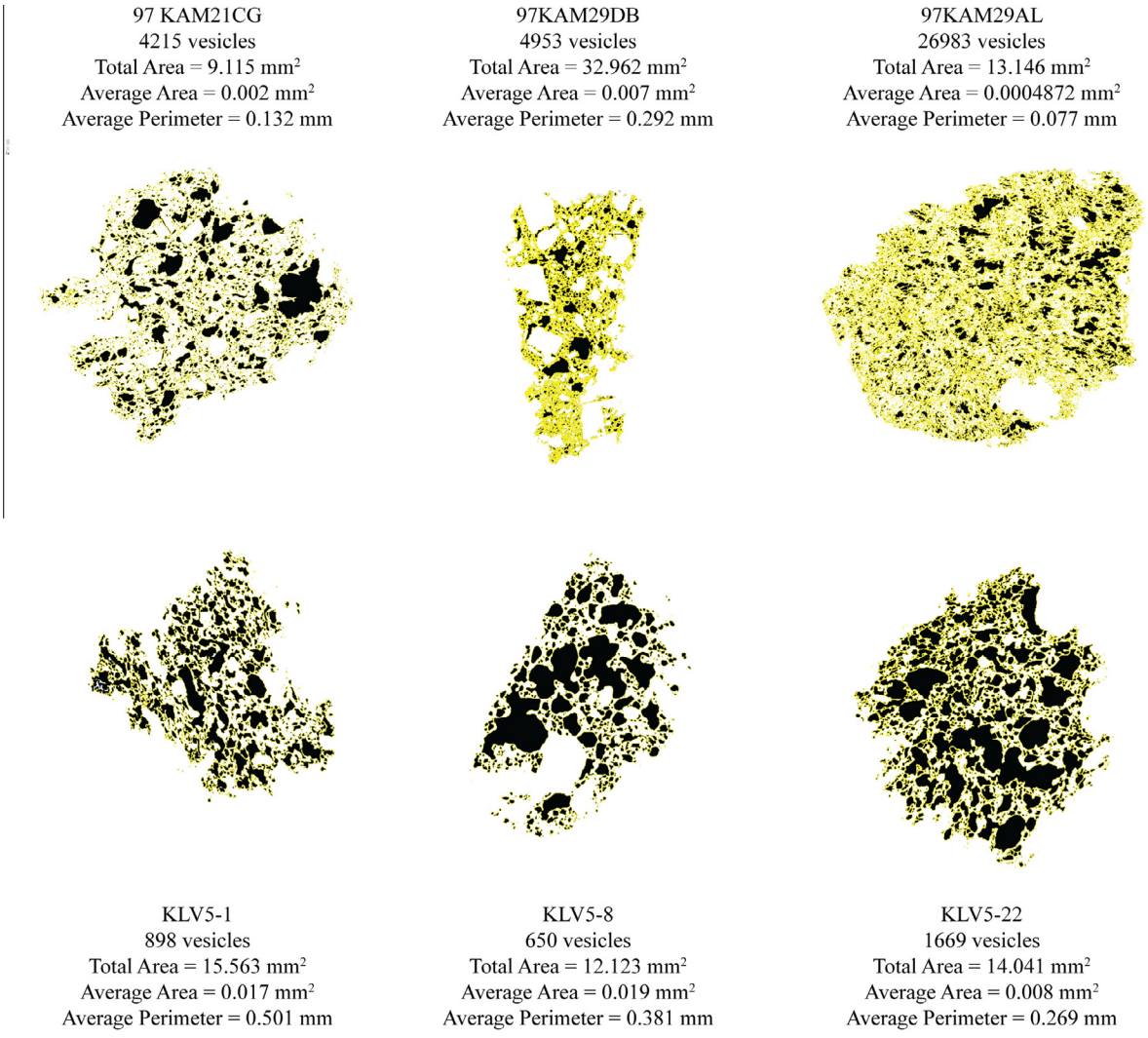

Fig. 6. Results from ImageJ analyses of the black and white images of each tephra clast (see Fig. 5) showing the number, area, and perimeter of the vesicles. Each vesicle counted and analyzed by ImageJ is outlined in yellow. (For interpretation of the references to color in this figure legend, the reader is referred to the web version of this article.)

(Fig. 9a). The only exceptions are the glasses from Volcán de Fuego and Kelud, which both fall near the 1:1 line and are both located near the equator (Fig. 1). They therefore have heavier local precipitation δD (‰) similar to the range of δD (‰) values of mostly degassed magmas (Figs. 2, 9a). Thus, as is illustrated in Fig. 2, the two types of water mask each other. The recent ash that is far from the 1:1 line is from the Alaskan Mt. Spurr, which is located at a northern latitude (Fig. 1), and therefore has local δD (‰) values of precipitation that are significantly lighter than average degassed magmas. This is also true for all Holocene Kamchatkan scoria and ash studied by us (Figs. 1, 9a, 10a). After applying the magmatic water correction, the mafic glasses fall within an average of 13‰ of the 1:1 line, now deviating an average of 43‰ less from the 1:1 line than they did prior to the magmatic water correction (Figs. 9 and 10). It should be noted that deviations from the 1:1 line also reflect our choice of δD, which we took from a global dataset rather than year-long averaged measurements that would have been more appropriate in this case, which is still possible to do in the future.

A natural experiment of secondary hydration of basaltic tephra is provided by the δD values of multiple tephra layers from Klyuchevskoy volcano in Kamchatka (0.05–7.3 ka), which lie above the 1:1 line prior to any magmatic water correction (Fig. 9a). Despite the fact that the majority of the water in the Klyuchevskoy glasses is higher δD undegassed magmatic water, we observe that the total water is increasing slightly, and the δD (‰) values are gradually decreasing with the increasing age of the tephra (Figs. 8, A2). This indicates a slow process of rehydration of up to 0.6 wt.% H_2O_t at 7.3 ka. After applying the correction, there is an average of 60‰ less deviation from the 1:1 line (Fig. 9b).

Water extracted from the postglacial 7.7 ka Mt. Mazama glasses and other Holocene felsic glass (0.3–10 ka) are, on average, within ~15‰ of the 1:1 line prior to the magmatic

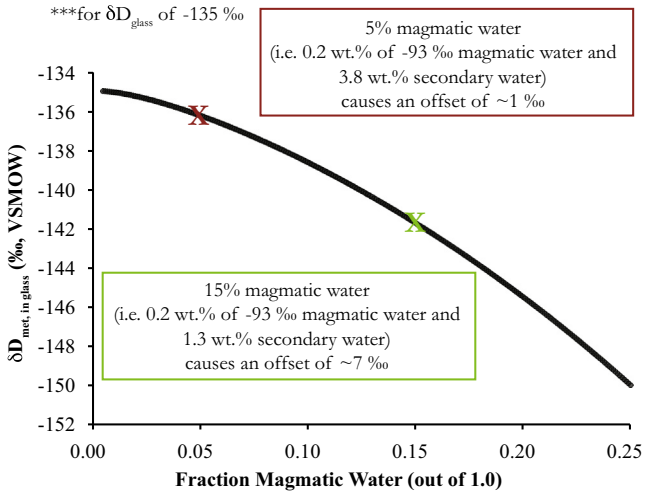

Fig. 7. Relationship between the amount of primary magmatic water left in the glass and the δD of the total water (secondary and primary) as determined by TCEA, based on Eqs. (2) and (3). We do not factor in the variations in OH^- and H_2O_{mol}. For this calculation, we varied the δD of the primary magmatic water with the H_2O_t wt.% of the primary magmatic water during degassing, based on degassing trends of Newman et al. (1988) and Castro et al. (2014), using the equation:

$$\delta D_{mag} = 13.8 \ln(H_2O_{t,mag}) - 71 \quad (4)$$

where δD_{mag} is the δD of the magmatic water during degassing in ‰, and $H_2O_{t,mag}$ is the wt.% H_2O_t of the magmatic water. Given the δD_t that is output by the TCEA results, we calculate the offset produced by the residual magmatic water on the actual δD of the secondary water, assuming there is no shift in the δD of the primary magmatic water during secondary hydration. The plot here shows actual δD_{met} waters if the δD_t value is −135‰ for different fractions of magmatic water (out of 1.0), and provides the necessary shift in δD values needed to obtain the actual δD_{met} value.

water correction (Fig. 9a). Following the magmatic water correction, the data are within an average of 4‰ of the 1:1 line. The lesser improvement in fit (although still significant) between the mafic and felsic samples is due to the difference in percentage of magmatic water, where the mafic tephra have a higher percentage of magmatic water than the secondarily hydrated felsic tephra. Although the improvement is smaller in the felsic samples, the magmatic water correction still creates an improvement in the correlation between the water in the glass and the surrounding meteoric water (Figs. 9 and 10).

When splitting the glass samples into low water concentration (<1.5 wt.% H_2O_t) and high water concentration (>1.5 wt.% H_2O_t) sets, there was an average of 46‰ less deviation from the expected δD_{met} value for the low water concentration samples and an average of 7‰ less deviation for the high concentration samples following the correction. This separation of water concentrations is also nearly represented by a separation of mafic versus felsic glasses, where only one rhyolite fell into the low water category (0.3 ka Opala) and three andesites (Rungwe and Kizimen) fell into the high water category, due to the tendency for rhyolites to become hydrated more rapidly.

4.2.1. Fractionation between meteoric water and volcanic glasses of mafic and felsic composition

We compare the D/H of water from our analyses to the local D/H of precipitation for each glass to calculate the fractionation between meteoric water and mafic and felsic glasses in varying climatic regions (Fig. A3). To do this, we utilize our magmatic corrected δD values and compare these values to the local δD of precipitation from Bowen and Revenaugh (2003) and Bowen (2015). We conduct this exercise separately for mafic and felsic glasses, and also for regions with different climates (hot/cold and wet/dry). We report fractionations as $10^3 \ln\alpha_{glass\text{-}water}$, where:

$$\alpha_{glass-water} = \frac{(1000 - \delta D_{glass})}{(1000 - \delta D_{water})} \quad (5)$$

glass designates the D/H ratio of water extracted from volcanic glass and water designates the D/H ratio of liquid meteoric water.

We determine an average global $10^3 \ln\alpha_{glass\text{-}water}$ of −33‰ (±15‰; 1 s.d.) for all our hydrated felsic glasses, in which we include glasses older than 2.0 ka with water concentrations greater than 1.5 wt.% (Fig. A3). This value is similar to the $10^3 \ln\alpha_{glass\text{-}water} = -34$‰ from Friedman et al. (1993a), and illustrates the kinetic fractionation that occurs during the addition of water into volcanic glass, where the lighter isotope (hydrogen) diffuses faster than the heavier isotope (deuterium). However, it is curious that Friedman et al. (1993a) did not conduct a magmatic correction on their glasses. Their method, however, utilized water contained within hydrated glass spheres from volcanic eruptions, and compared the δD of the liquid water within the hollow sphere (presumed to represent environmental water) to the δD of the water extracted from the glass to determine their $10^3 \ln\alpha_{glass\text{-}water}$. Their difference in methodology leads to differing assumptions and causes our comparisons to become difficult. If we include all felsic

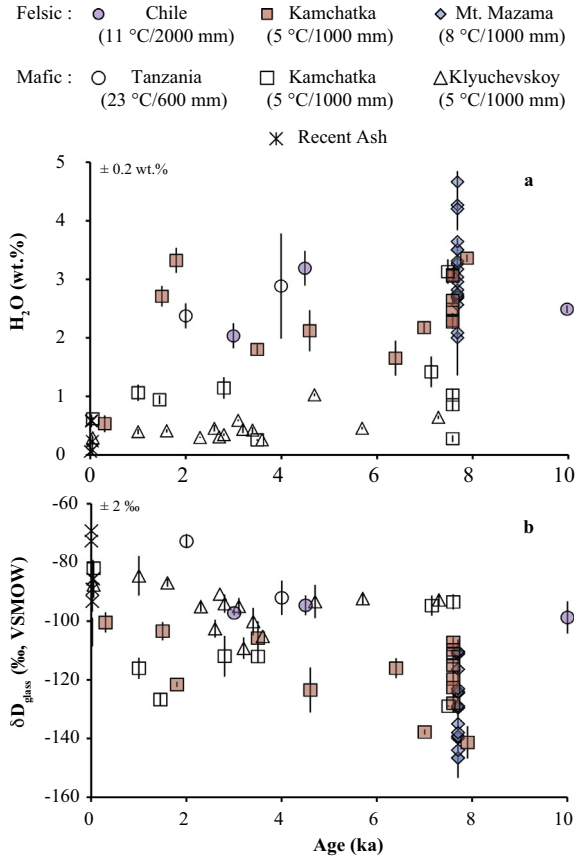

Fig. 8. Water concentration (wt.%) and δD (‰) trends of water in glass with time (error bars illustrate ±1 s.d.). The mean annual temperature (MAT) in °C and average annual precipitation in mm are listed for each region in the legend. (a) H_2O_t (wt.%) trends for mafic and felsic tephra with age. This plot illustrates a distinction between the hydration rate of basaltic tephra (slower) and rhyolitic tephra (faster), where rhyolitic tephra already contains above 1.5 wt.% H_2O_t after ~1500 years. (b) δD_{glass} trends for mafic and felsic tephra with age. Since the majority of tephra around the world are hydrated with meteoric water with a lower δD (‰) than the residual primary magmatic water (when factoring in the fractionation between water in glass and meteoric water from Friedman et al. (1993a)), the predominant trend shown during secondary hydration is a decrease in the δD (‰) of the water in the glass. This causes felsic (hydrated) tephra to have a lower δD (‰) value after a few thousand years than the majority of the mafic (not as hydrated) tephra. The ±2‰ δD and ±0.2 wt.% H_2O_t on the *y*-axes illustrate the typical reproducibility of our TCEA.

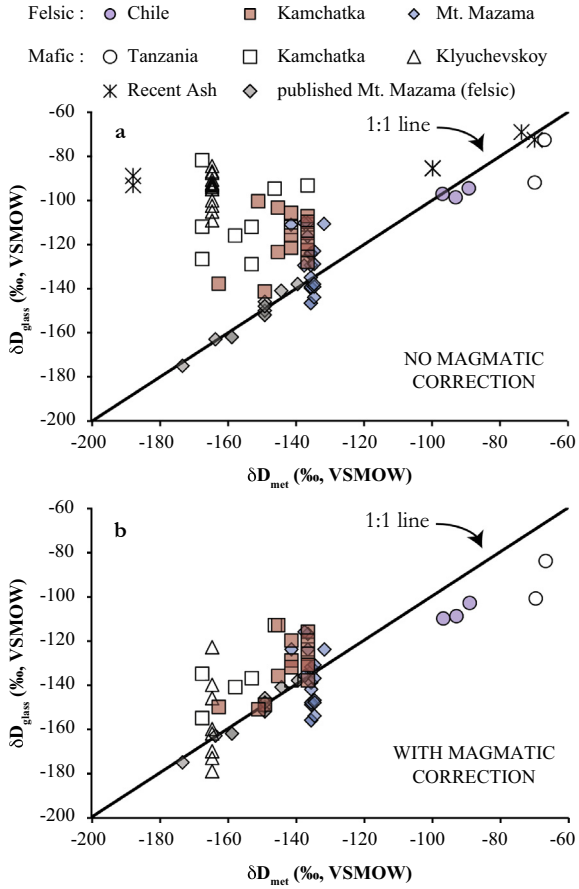

Fig. 9. δD_{glass} (‰) in comparison to local δD_{met} (‰). The 1:1 line compares the δD (‰) of the water extracted from the volcanic glass (our analyses) to the δD (‰) of current local meteoric water based on interpolated data from waterisotopes.org (Bowen and Revenaugh, 2003; Bowen, 2015). The fractionation between water in glass and meteoric water (Friedman et al., 1993a) has already been taken into account. (a) Results when an average magmatic water δD (‰) value is not excluded from the δD_{glass} (‰) value. Results here show an average offset of +24‰ from current local meteoric waters for all data. (b) Results showing the improved correlation when the average magmatic water δD (‰) value is removed from the δD_{glass} (‰) value. The average offset for both mafic and felsic glasses following the magmatic water δD (‰) correction is +4‰. Glasses used to create the magmatic correction and glasses with water concentrations less than the magmatic correction are excluded from (b). Published Mt. Mazama data is from Friedman et al. (1993b).

glasses, except those used in the magmatic water correction, the $10^3\ln\alpha_{glass\text{-}water}$ is slightly smaller at −31‰ (±16‰; 1 s.d.). Fig. A3 also illustrates the $10^3\ln\alpha_{glass\text{-}water}$ of −20‰ (±17‰; 1 s.d.) for all our felsic glasses prior to the magmatic correction, which does not agree with the $10^3\ln\alpha_{glass\text{-}water}$ of Friedman et al. (1993a). We also find variations in the $10^3\ln\alpha_{glass\text{-}water}$ value when we split these same data up into separate climatic regions. The average $10^3\ln\alpha_{glass\text{-}water}$ for the cold and wet climate of Kamchatka (MAT of ~5 °C and average annual precipitation of ~1000 mm) is −20‰ (±11‰; 1 s.d.). The average $10^3\ln\alpha_{glass\text{-}water}$ for the warm and wet climate of Chile (MAT of ~11 °C and annual precipitation of ~2000 mm) is −50‰ (±2‰; 1 s.d.). We also include the Pacific Northwest of the United States (Mt. Mazama pumices), which covers a range of climatic settings. Most of the pumices were collected near Crater Lake National Park, which is located in a cold (~8 °C MAT) and wet (~1000 mm annual precipitation) environment. The average $10^3\ln\alpha_{glass\text{-}water}$ for these pumices is −37‰ (±15‰; 1 s.d.). Two of the Mt. Mazama samples were collected farther to the east (Mazama-WMC, 2014MM-1), in a dryer setting (~300 mm annual precipitation), and yield an average $10^3\ln\alpha_{glass\text{-}water}$ of −29‰ (±28‰; 1 s.d.). Although we find a similar average fractionation to Friedman et al.

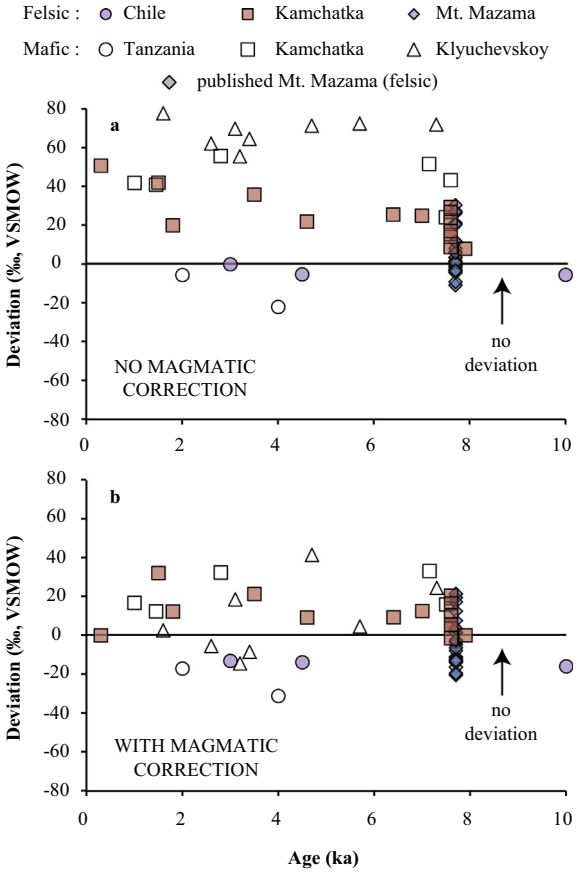

Fig. 10. Deviation from the δD (‰) of local meteoric waters in relation to the age of the glass. The black line running through 0‰ designates no deviation from the δD of local meteor water (Bowen and Revenaugh, 2003; Bowen, 2015), after taking into account the Friedman et al. (1993a) fractionation between water in glass and meteoric water. (a) Results when an average magmatic water δD (‰) value is not excluded from the δD_{glass} value. Nearly all δD glass data fall above the correlation line. (b) Results showing the improved correlation when the average magmatic water δD (‰) value is removed from the δD_{glass} value. The correction causes more data to fall near the correlation line. Glasses used to create the magmatic correction and glasses with water concentrations less than the magmatic correction are excluded from part (b). Published Mt. Mazama data are from Friedman et al. (1993b).

(1993a) for all of our tephra, we observe a large variation in our $10^3\ln\alpha_{glass\text{-}water}$ averages, represented here as large standard deviations. In addition, counter to what would be expected, we see larger fractionations in warm and wet settings, although we only have 3 samples from a warm and wet region, and two from a dry region, which are not significant enough to build a final conclusion.

Our global data set for the hydrated mafic glasses is significantly smaller than that for the felsic glasses (Fig. A3). If we only include glasses with >1.5 wt.% H_2O_t that are older than 2000 years, we have just three glasses to create our average $10^3\ln\alpha_{glass\text{-}water}$ of −45‰ (±27‰; 1 s.d.). We do not consider three glasses significant enough to make a final conclusion on mafic fractionations. Our global average for all mafic glass $10^3\ln\alpha_{glass\text{-}water}$ is −23‰ (±23‰; 1 s.d.), which is smaller than our (and Friedman et al., 1993a) estimate for the felsic $10^3\ln\alpha_{glass\text{-}water}$. Unlike for the felsic glasses, we find the $10^3\ln\alpha_{glass\text{-}water}$ of the larger data set of the mafic glasses that has been corrected for residual magmatic water to be more robust. This is due to there being only a few hydrated mafic glasses in this study. If we determine the $10^3\ln\alpha_{glass\text{-}water}$ for the mafic glasses, prior to the magmatic correction, it becomes +19‰ (±32‰; 1 s.d.), which is likely due to the prevalence of magmatic water in the mafic glasses with heavier δD values, signifying the importance of the magmatic correction. Similar to the felsic glasses, we compare fractionations between regions of cold and wet versus hot and dry climates. For the cold and wet region of Kamchatka, the average $10^3\ln\alpha_{glass\text{-}water}$ is −19‰ (±19‰; 1 s.d.), and for the hot and dry region of Tanzania (MAT of ~23 °C and annual precipitation of ~600 mm) the average $10^3\ln\alpha_{glass\text{-}water}$ is −60‰ (±11‰; 1 s.d.). This indicates a similar trend of greater fractionations for hot and dry climates in the mafic glasses. Also similar to the felsic trend, we have minimal samples to base this trend on, and therefore, it is uncertain if this trend is significant.

4.3. Hydration of basalt versus rhyolite

There is a clear distinction between the hydration rates of basalt and rhyolite glass (Fig. 8). This difference is likely due either to the difference in diffusion rates of water into basaltic and rhyolitic glass, differences in vesicularities, or both. Due to the long time (1000s of years) needed for room temperature hydration, there are no experiments on rates of room temperature hydration of basalt or rhyolite tephra. Therefore, experimental data for rhyolite and basalt diffusivities only go to 400 °C (e.g. Zhang and Behrens, 2000).

As we documented above (Fig. 4, Table 4), rhyolitic tephra has more bubbles per unit area (736 mm^{-2}) relative to basalts and andesites (27–161 mm^{-2}). The important implication of this difference in numbers of bubbles is that the reactive surface area of the glass increases with an increase in bubble frequency, which we examine further below.

4.3.1. Hydration rates of coeval tephra across differing climates

We compare the H_2O_t of tephra of similar age and relative vesicularities across different climatic regions and do not observe consistent differences in hydration rates of felsic or mafic tephra (Fig. 8). In terms of the felsic samples, the Chilean glasses were hydrated in the warmest and wettest climate and we compare these tephra to the cooler climates of Kamchatka and Oregon (United States). We compare the youngest Chilean glass (CLD064B; 3 ka) with a similarly aged Kamchatkan glass from Opala (98–33/2) that has similar vesicularity (Table 3) and find similar water concentrations. However, when we compare an older Chilean glass (CLD155A) with a similar vesicularity to the 4.6 ka Optr glass (98KAM2.3), we do not find similar water concentrations (3.2 wt.% H_2O_t relative to 2.1 wt.% H_2O_t). Based on the random differences in water concentrations between the few tephra of the warm and wet Chilean climate that we can compare to specific Kamchatkan samples,

we cannot conclude that there are any consistent differences in rates of hydration for felsic glasses of differing climates (i.e. cold versus warm). However, we only have a few warm samples to work with, and therefore more research should be done to clarify these results.

We can utilize a similar comparison of the mafic Tanzanian glasses, which were hydrated in a warmer and dryer climate to the cold and wet climate of the Kamchatkan glasses (Fig. 8a; Table 3). However, specific age and vesicularity comparisons are difficult, due to the few samples we have from warm and dry climates. The 2.0 ka Rungwe tephra (KF155D) is bracketed by the 1.0 and 2.8 ka Shiveluch glasses (96025/4 and 97051/2), which both have lower relative vesicularities and lower water concentrations. We compare the older (4.0 ka) Rungwe glass (KF149B) to the 2.8 ka Shiveluch tephra and the 7.5 ka Kizimen tephra (80013/4), which have lower relative vesicularities, and lower and higher water concentrations, respectively. Again, based on the random differences in total water concentrations for both the mafic and felsic glasses that we see here, there does not appear to be any consistent difference in hydration rates for glasses hydrated in different climatic regions. However, we don't have very many dry climate samples to work with, and more research should be done to clarify these results.

4.4. Simplified model for diffusion of water through vesicular glass

A longstanding experimental challenge is the measurement of the diffusivity of water in volcanic glass at ambient temperature. Because the rate of diffusion is so slow, and therefore difficult to investigate with experiments, one approach is to measure the thickness of hydration rinds on obsidians of known age (e.g. Anovitz et al., 2004). In this section, we develop a complementary approach in which we model the hydration versus time data presented in Fig. 8 to obtain an order-of-magnitude estimate of the low-temperature diffusivity of H_2O_t in both vesicular rhyolite and basaltic scoria.

The key observations we focus our attention on are: (1) the H_2O_t in rhyolitic pumices increases between 0 and 2 ka; (2) most of the basaltic scoria are considerably less hydrated than their rhyolitic counterparts; (3) there is no systematic relationship between age and H_2O_t in rhyolitic or basaltic tephra older than 2 ka; and (4) basaltic scoria older than 1.5 ka are more hydrated than modern basalts. It is important to note at the outset that we do not have independent constraints on the solubility of water in basalt and rhyolite at low temperature, and we make the assumption that the solubility of water in mafic and felsic glasses is similar.

We model the diffusive influx of water into a glass wall between two bubbles in 1D to estimate the rate at which the glass wall becomes hydrated as a function of the diffusivity of water and average vesicle wall thickness (Fig. 11a and b). An alternative way to think of this is that we are representing a square slab of ash with a thickness that is represented by the bubble wall thickness. At an equivalent mass, thinner-walled tephra clasts will have a greater surface area. In the model, the glass wall initially has 0.1 wt.% water and we assume a 5 wt.% fixed concentration of water at the boundaries, which is near our highest water content after 10,000 years. The fixed concentration boundary conditions imply that the clast as a whole is highly permeable such that environmental water can penetrate into most of the pores. Although the water concentration of 5 wt.% at the boundaries is fixed, the diffusivity within the model varies with time as the water concentration changes.

The two parameters in the model that determine the rate of hydration versus time are (1) the length that water has to travel to hydrate the glass (average bubble wall thickness) and (2) the diffusivity of water. Because hydration rinds are observed to have relatively sharp boundaries due to the water-concentration dependence of diffusivity (Eq. (1) and surrounding discussion), similar to what is seen in studies involving glass corrosion (e.g. Gin et al., 2013; Steefel et al., 2015), we adopt the formulation for the water concentration dependent rhyolite diffusion equation from Zhang and Behrens (2000):

$$D_{H_2O_t} = X\exp(m)\left\{1+\exp\left[56+m+X\left(-34.1+\frac{44,620}{T}+\frac{57.3P}{T}\right)-\sqrt{X}\left(0.091+\frac{4.77\times10^6}{T^2}\right)\right]\right\} \quad (6)$$

where D is a water concentration diffusion coefficient in $\mu m^2/s$ for molecular water, $m = -20.79–5030/T-1.4P/T$, T is the temperature in Kelvin, P is the pressure in MPa, and X is the mole fraction of H_2O_t on a single oxygen basis. This equation, however, is based on experimental and literature data at temperatures >400 °C, and we therefore only utilize it for its dependence on water concentrations at these higher temperatures, while making the assumption that the functional form is still the same at much lower temperatures. As water diffusivity in glass strongly increases with water concentration (Zhang and Behrens, 2000), we first use the slowest water diffusivity at 0.1 wt.% as the rate-limiting factor for water diffusion. Furthermore, since diffusion is much slower at 25 °C, we scale the diffusivity by a constant prefactor, which turns out to be between 10^{-8} and 10^{-10}, in order to match the trend of increasing H_2O_t with age from our data. The constant prefactor is the only free parameter, as we use average bubble wall thicknesses inferred from the imaged tephra clasts in Fig. 4 and Table 4.

Fig. 11c–d shows an example diffusion simulation for the 7.6 Kurile Lake rhyolite. The initial diffusivity (at 0.1 wt.% H_2O_t) required to yield an average water concentration of 2.3 wt.% after 7.6 ka is on the order of 10^{-4} μm^2/year. Hereafter, we report diffusivities at 0.1 wt.% water because this is the value that governs the length scale of diffusion according to Eq. (1). The value of 10^{-4} μm^2/year for the Kurile Lake rhyolite is somewhat sensitive to the solubility of water, or the assumed concentration of water at the boundary. For example, assuming a boundary concentration of 3 wt.% increases the diffusivity needed to match 2.3 wt.% at 7600 years by one order of magnitude to 10^{-3} μm^2/year.

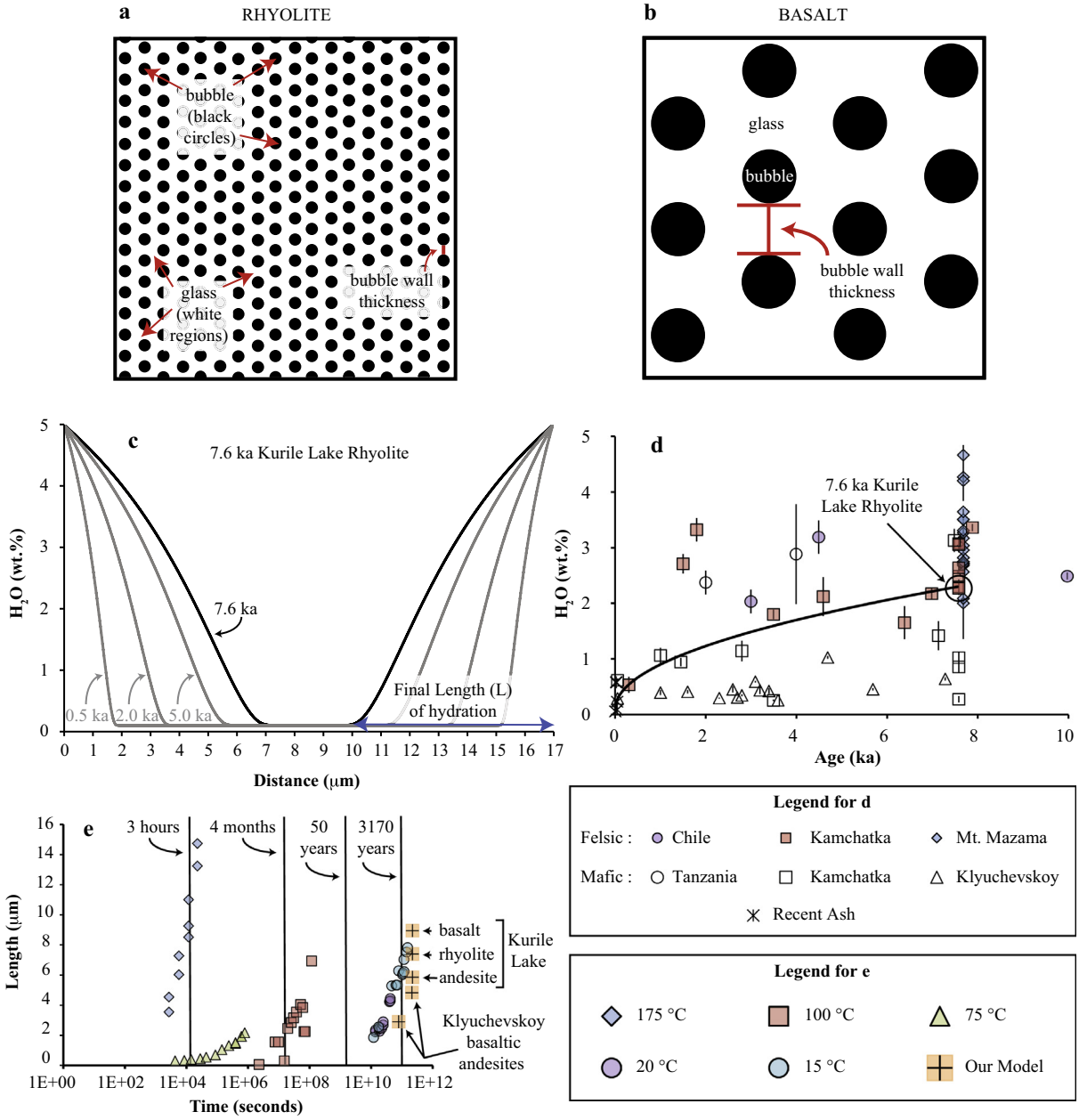

Fig. 11. Comparison and explanation of our model results for water concentration dependent diffusion. (a and b) illustration of the hexagonal close-packing assumption that we utilize in our vesicle and glass layout for our model. The difference between (a) and (b) illustrates the typical difference in bubble wall thicknesses between rhyolite (a) and basalt (b) tephra. (c) Example of our model results for 97KAM29AL (7.6 ka Kurile Lake Rhyolite). 97KAM29AL has an average bubble wall thickness of 17 μm (shown on the *x*-axis). At the start of the model run, the entire bubble wall has 0.1 wt.% H_2O_t, with 5 wt.% H_2O_t at the boundaries. As hydration proceeds (0.5–7.6 ka shown here), the hydration front produces a 'bulldozing effect' that steadily progresses into the center of the bubble wall, as is shown in the 0.5, 2.0, 5.0, and 7.6 ka markings in gray. The length of hydration (L) for each of our tephra samples was calculated by subtracting the average bubble wall thickness (17 μm here) by the distance to the 0.1 wt.% non-hydrated region of the bubble wall (9.6 μm after 7600 years here). (d) To determine the proper distance needed for hydration, the known bubble wall thickness from the SEM images was entered into our model (17 μm for 97KAM29AL), along with the known age (7.6 ka for 97KAM29AL), and the diffusivity constant was adjusted until the known water concentration from the TCEA analyses was obtained (2.3 wt.% here). This is shown here by the trend of increasing water with time to end at 2.3 wt.% H_2O_t after 7600 years. (e) Results show that there is a decrease in hydration rate with a decrease in temperature and that our model results are similar to those for natural rhyolitic glass hydration at 15 and 20 °C. This is shown by our tephra (from Kurile Lake and Klyuchevskoy) having similar lengths of hydration for similarly aged samples at 15 and 20 °C. Given the slightly lower temperature of our Kamchatka samples (~5 °C mean annual temperature), it is reasonable that our samples have a slightly slower hydration rate than the samples at 15–20 °C. We did not determine the hydration distance of KLV5-1 (0.05 ka Klyuchveskoy scoria) based on its young age, and likely negligible secondary hydration. Prior studies are from Friedman et al. (1966; 100 °C), Mazer et al. (1991; 175 °C), Anovitz et al. (2004; 75 °C), Riciputi et al. (2002; 20 °C), and Eerkens et al. (2008; 15–20 °C). Higher degree temperatures listed in the legend are approximate and based on the average temperature for the study.

We applied the same approach to modeling each of the six imaged tephra clasts for which we have SEM images of bubble wall thickness. The youngest Klyuchveskoy basaltic andesite (KLV5-1, 0.05 ka) was not included in this analysis, since the water in this clast is likely all magmatic water, based on its young age, high δD, and low water concentration. All diffusivities for these samples are within the same order of magnitude (10^{-4} μm^2/year; results not shown). Lengths that we determine from our model produce similar rates of secondary hydration (1–10 μm/1000 years) as were documented by Friedman et al. (1966). Fig. 11e shows the length of hydration taken from the modeled 1D diffusion profile versus age for each of the five samples. Also shown is the temperature-dependence of the rate of hydration as determined from several different studies, and the results are generally consistent except for the discrepancy between 75 and 100 °C. The results from our five samples compare favorably to samples that were naturally hydrated at 15–20 °C. The slightly slower rate of hydration for our tephra samples from Kamchatka could be attributed to a number of factors, but it is noteworthy that the mean annual temperature of Kamchatka is about 5 °C, which could theoretically cause slightly slower hydration than at 15–20 °C.

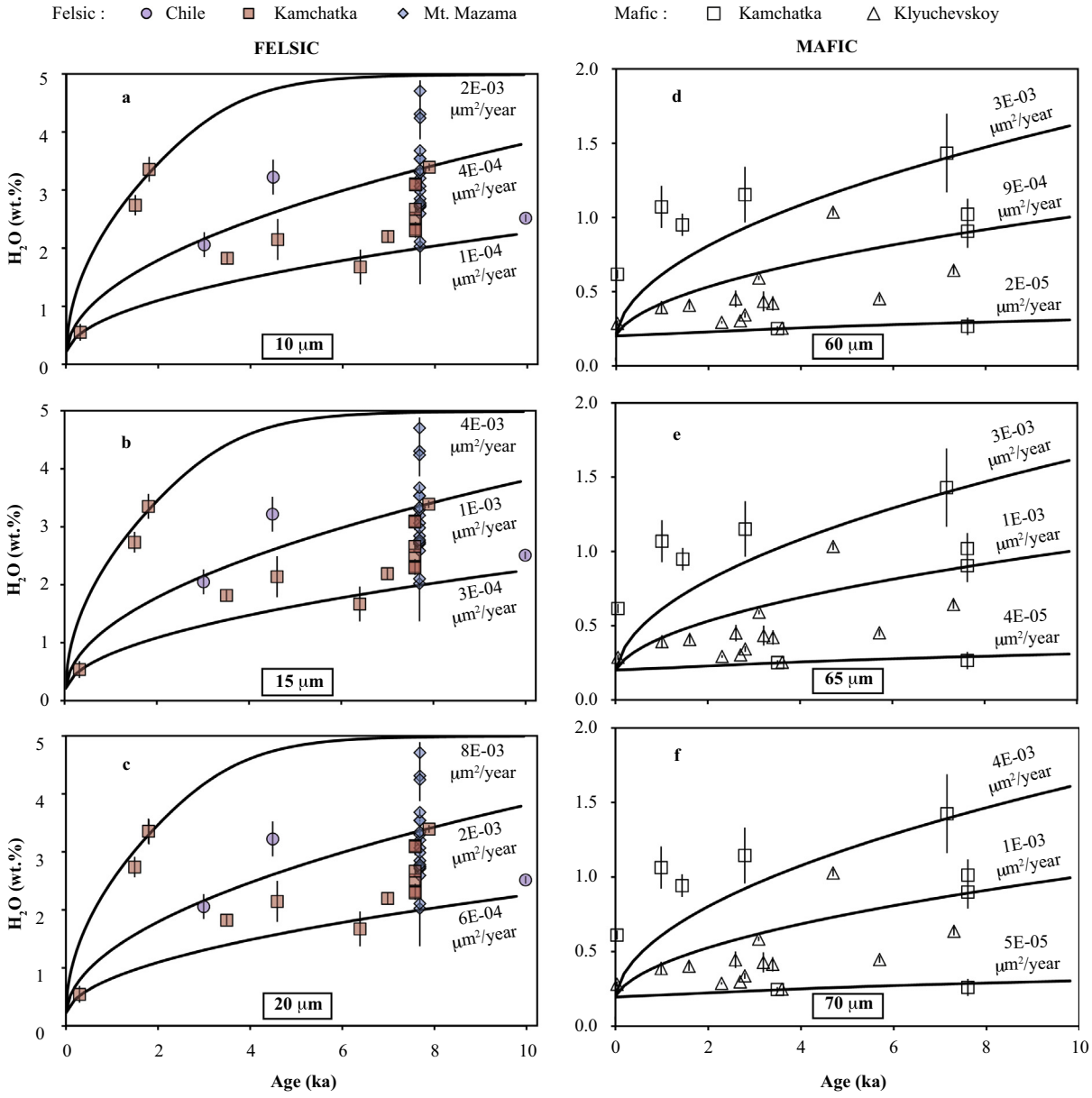

Fig. 12. Modeling results from our diffusion code for felsic (a–c) and mafic (d–f) glasses in comparison to our data for water concentration versus age (error bars illustrate ±1 s.d.). For the felsic glasses, the bubble wall thickness was varied between 10, 15, and 20 μm, and the diffusivities were subsequently varied at each of these average bubble wall thicknesses until the trend lines matched our data. For the basalts, the bubble wall thickness was varied between 60, 65, and 70 μm. Diffusivities listed in the figure are the initial diffusivity at 0.1 wt.% H_2O_t.

Fig. 12 shows the tradeoff between diffusivity and vesicularity (or average bubble wall thickness) for the entire sample set, with the exception of three mafic samples with >2 wt.% water. For the felsic tephra, we vary the bubble wall thicknesses from 10 to 20 μm, based on the Kurile Lake rhyolite. For the mafic tephra, we vary the bubble wall thicknesses from 60 to 70 μm, based on the average bubble wall thicknesses for the imaged mafic tephra (Fig. 12). Each panel corresponds to a specified bubble wall thickness, and the curves that bracket the data represent different diffusivities. Based on this comparison, we find that diffusivities for both felsic and mafic glass range between 10^{-3} and 10^{-5} μm^2/year, with the upper bounds for both the felsic and mafic glass having diffusivities $\sim10^{-3}$ μm^2/year, the lower bound of the felsic glasses having diffusivities of $\sim10^{-4}$ μm^2/year, and the lower bound of the mafic glasses having diffusivities $\sim10^{-5}$ μm^2/year (Fig. 12).

In Fig. 12, the symbols represent geographic setting. In Fig. 13, we use symbols corresponding to relative vesicularity. The first thing to note is that the highest water content samples have high vesicularity, whereas the lowest water content samples span the full range from low to high vesicularity. This is true for both mafic and felsic samples. Note that we plot results for a larger range of bubble wall thicknesses than used in Fig. 12, which is necessary to fit the highest water content mafic samples. When comparing diffusivities, we still see no significant difference between mafic versus felsic glasses at low temperatures. Therefore, we conclude that rhyolite tephra becomes hydrated more rapidly on average than basaltic tephra because of higher reactive surface area arising from higher vesicularity and smaller average bubble wall thickness. Although the vast majority of the felsic tephra hydrate faster than the mafic tephra in this study, there are three mafic samples (the 2.0 and 4.0 ka Rungwe glass and the 7.5 ka Kizimen glass) that became hydrated at a similar rate to some of the felsic tephra. These tephra all have higher vesicularities than most other mafic tephra, which provides a larger surface area for hydration (Table 3). Rust and Cashman (2011) compiled the relative bubble number densities of basalt and rhyolite tephra and showed that rhyolite tephra have consistently higher bubble number densities (and therefore surface areas), regardless of the mass eruption rate, than mafic tephra. Their compilation also showed that mafic tephra have bubble number densities that increase with increasing mass eruption rates, which correlates with our results of only a few of the mafic tephra being hydrated at similar rates to the felsic tephra.

Furthermore, when plotted versus age, there is a range of hydration rates for basaltic glasses, with the Klyuchevskoy basalts being hydrated at the slowest rates (Fig. 8). There are two potential explanations for this difference: (1) the lower explosivity of the Klyuchevskoy eruptions translates to fewer vesicles, and therefore, thicker bubble walls (Table 4; Figs. 4–6). This would cause water to take longer to penetrate through all the glass; and/or (2) the presence of microlites causes water to diffuse through longer effective pathways, and thus slowly through the pyroclast. Both thicker bubble walls and abundance of microlites have been documented in the Klyuchevskoy tephra, which explains the unusually slow hydration rate of the Klyuchevskoy tephra.

4.4.1. Modeling D/H diffusion during secondary hydration

To further understand the δD trends of secondary hydration, we created a similar code to incorporate the D/H trends during diffusion of water into volcanic glass at ambient temperature for the 7.6 ka Kurile Lake rhyolite (97KAM29AL) from Kamchatka, Russia. We use the same

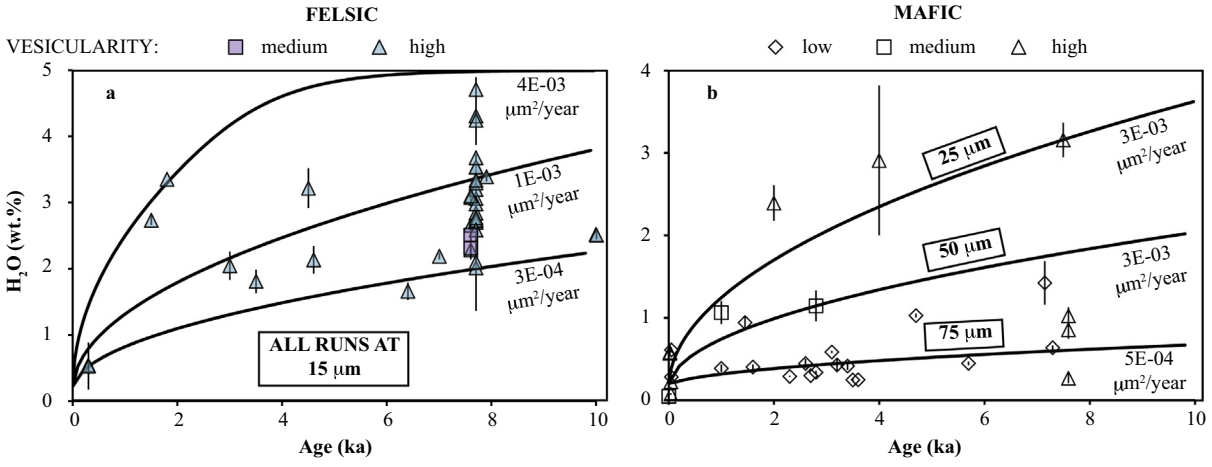

Fig. 13. Modeling results from our diffusion code for felsic (a) and mafic (b) glass against our data for water concentration versus age (error bars illustrate ±1 s.d.). Vesicularities were split into three groups: (1) highly vesicular samples, with relative vesicularities from 7 to 10; (2) moderately vesicular, with a relative vesicularity of 5; and (3) low vesicularity samples, with relative vesicularities from 1 to 4. Relative vesicularities are listed in Table 3. Given the vesicular nature of the felsic samples, model runs were only conducted at 15 μm bubble wall thickness. Based on the wide range of vesicularities for the mafic samples, highly vesicular data were matched to 25 μm bubble walls, moderately vesicular data were matched to 50 μm bubble walls, and low vesicularity data were matched to 75 μm bubble walls. Results here show similar orders of magnitude diffusion for mafic and felsic samples, when relative vesicularities are accounted for.

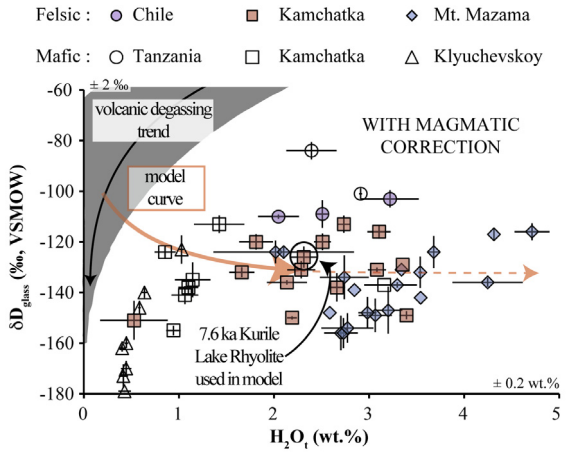

Fig. 14. Modeling results from our δD diffusion code. The δD_{glass} values in this figure are magmatic corrected (error bars illustrate ±1 s.d.). Note the lower δD values for the δD_{glass} data, and the similarity between the model curve and our schematic curve in Fig. 2. The model was run up to the 2.3 wt.% H_2O_t for the 7.6 ka Kurile Lake rhyolite (97KAM29AL) using the local precipitation annual δD (‰) value from waterisotopes.org (Bowen and Revenaugh, 2003; Bowen, 2015), along with the fractionation between water in glass and meteoric water (Friedman et al., 1993a). The continued dashed line following the solid model curve is a projected continuation of the model trend. The ±2‰ δD and ±0.2 wt.% H_2O_t on each axis illustrate the typical reproducibility of our TCEA.

model set up from the water-based diffusion model discussed above, except the starting conditions are now based on the relative deuterium concentrations from the δD of our magmatic correction (−83‰) at 0.1 wt.% H_2O_t, and the boundary conditions are based on the current local δD of precipitation (−107‰) from Bowen and Revenaugh (2003) and Bowen (2015), while including the fractionation between water in glass and meteoric water from Friedman et al. (1993a) for a δD boundary condition of −137‰. For the purpose of this model, we assumed that water addition and D/H exchange coincide. We compare this model to the δD values of our samples that have been magmatic corrected (Fig. 14), and note that our model produces similar results to the schematic curve from Fig. 2, and the magma corrected δD value of our 7.6 ka Kurile Lake rhyolite. This correlation illustrates both the appropriateness of our model, and the ability to obtain similar δD values for water extracted from volcanic glass (following a magmatic correction) and the local δD of precipitation.

5. CONCLUSIONS

(1) We demonstrate the characteristics of the hydrogen isotope variations of secondary hydration of volcanic glass, which illustrates a decrease in the δD value with increasing water in nearly all environments except equatorial.

(2) We propose a correction for pre-existing undegassed magmatic water when determining paleoenvironments, where younger tephra from the same section can be used to constrain the δD and concentration of residual magmatic water of older tephra clasts. If younger tephra from the same section are not available, our average δD of −83‰ and H_2O_t of 0.32 wt.% still aid in the correlation between water extracted from secondarily hydrated volcanic glass and local meteoric waters.

(3) We show that δD values of water in felsic volcanic glass (⩽∼10,000 years), when compared to present meteoric water, yield uncertainties of ±4‰ from the current δD of meteoric water after a magmatic correction.

(4) Following our magmatic correction, we calculate $10^3\ln\alpha_{glass\text{-}water}$ values that average −33‰ for hydrated felsic glasses, which is similar to the $10^3\ln\alpha_{glass\text{-}water}$ value determined by Friedman et al. (1993a). We also identify a smaller average $10^3\ln\alpha_{glass\text{-}water}$ for all mafic glasses across differing climates of −23‰.

(5) We demonstrate that felsic glass typically becomes mostly hydrated after ∼1500 years with 1.5–3.5 wt.% H_2O_t, but mafic glass is typically still not hydrated beyond 1.5 wt.% H_2O_t even after 7000 years.

(6) When corrected for greater bubble frequency per unit area of rhyolites, we empirically estimate, using our tephrachronological sample set, that the diffusivity of water into felsic glass is within the same order of magnitude as mafic glass.

(7) We estimate the initial (at 0.1 wt.% H_2O_t) diffusion coefficient for water in felsic and mafic glass at ambient temperatures and pressures to be between 10^{-3} and 10^{-4} μm^2/year. This equates to a constant prefactor for the Zhang and Behrens (2000) rhyolite diffusion equation for temperatures above 400 °C that ranges between 10^{-8} and 10^{-10}, and provides similar rates of secondary hydration (1–10 μm/1000 years) determined earlier by Friedman et al. (1966).

ACKNOWLEDGMENTS

We thank David Sherrod for assistance with determining good sampling locations for Mt. Mazama ash and pumice around Oregon. We also thank Heather Wright for recently erupted samples from Indonesia, Caroline Gordon for Mt. Mazama samples from the Ochoco National Forest, and Karen Fontijn for samples from Chile and Tanzania. We would like to express our gratitude to Vera Ponomareva for fieldwork assistance and sharing samples from Kamchatka that were utilized in this research. We are also indebted to Gary Nolan and Jim Palandri for discussions and assistance with TCEA analyses. We would also like to thank Julie Chouinard for assistance with SEM imaging. A.N.S. owes a very large thank you to Dana Drew for assistance with fieldwork and sample collection, Danielle McKay for assistance with tephra sampling in central Oregon, and Randy Krogstad for assistance with the Matlab code. We also thank Carl Steefel and an anonymous reviewer for their constructive reviews and Marc Norman and Carl Steefel for editorial handling. This work was supported by the NSF [EAR/CAREER-844772], a Kleinman grant, and a grant from the Evolving Earth Foundation.

APPENDIX A. SUPPLEMENTARY DATA

Supplementary data associated with this article can be found, in the online version, at http://dx.doi.org/10.1016/j.gca.2016.07.010.

REFERENCES

Anovitz L. M., Elam J. M., Riciputi L. R. and Cole D. R. (2004) Isothermal time-series determination of the rate of diffusion of water in Pachuca obsidian. *Archaeometry* **46**, 301–326.

Anovitz L. M., Cole D. R. and Fayek M. (2008) Mechanisms of rhyolitic glass hydration below the glass transition. *Am. Mineral.* **93**, 1166–1178.

Anovitz L. M., Cole D. R. and Riciputi L. R. (2009) Low-temperature isotopic exchange in obsidian: implications for diffusive mechanisms. *Geochim. Cosmochim. Acta* **73**(13), 3795–3806.

Auer S., Bindeman I., Wallace P., Ponomareva V. and Portnyagin M. (2009) The origin of hydrous, high-$\delta^{18}O$ voluminous volcanism: diverse oxygen isotope values and high magmatic water contents within the volcanic reord of Klyuchevskoy volcano, Kamchatka, Russia. *Contrib. Mineral. Petrol.* **157**, 209–230.

Bindeman I. N., Kamenetsky V., Palandri J. and Vennemann T. (2012) Hydrogen and oxygen isotope behavior during variable degrees of upper mantle melting: example from the basaltic glasses from Macquarie Island. *Chem. Geol.* **310–311**, 126–136.

Bowen G. J. (2015) The Online Isotopes in Precipitation Calculator, version 2.2. http://www.waterisotopes.org.

Bowen G. J. and Revenaugh J. (2003) Interpolating the isotopic composition of modern meteoric precipitation. *Water Resour. Res.* **39**(10), 1299.

Braitseva O. A., Ponomareva V. V., Sulerzhitsky L. D., Melekestsev I. V. and Bailey J. (1997) Holocene key-marker tephra layers in Kamchatka, Russia. *Quatern. Res.* **47**, 125–139.

Cailleteau C., Angeli F., Devreux F., Gin S., Jestin J., Jollivet P. and Spalla O. (2008) Insight into silicate-glass corrosion mechanisms. *Nat. Mater.* **7**, 978–983.

Canavan R. R., Carrapa B., Clementz M. T., Quade J., DeCelles P. G. and Schenbohm L. M. (2014) Early Cenozoic uplift of the Puna Plateau, Central Andes, based on stable isotope paleoaltimetry of hydrated volcanic glass. *Geology* **42**, 447–450.

Cassel E. J., Graham S. A., Chamberlain C. P. and Henry C. D. (2012) Early Cenozoic topography, morphology, and tectonics of the northern Sierra Nevada and western Basin and Range. *Geosphere* **8**, 229–249.

Cassel E. J., Breecker D. O., Henry C. D., Larson T. E. and Stockli D. F. (2014) Profile of a paleo-orogen: high topography across the present-day Basin and Range from 40 to 23 Ma. *Geology* **42** (11), 1007–1010.

Castro J. M., Bindeman I. N., Tuffen H. and Schipper C. I. (2014) Explosive origin of silcic lava: textural and δD-H_2O evidence for pyroclastic degassing during rhyolite effusion. *Earth Planet. Sci. Lett.* **405**, 52–61.

Cerling T. E., Brown F. H. and Bowman J. R. (1985) Low-temperature alteration of volcanic glass: hydration, Na, K, ^{18}O, and Ar mobility. *Chem. Geol.* **52**, 281–293.

Crovisier J., Advocat T. and Dussossoy J. (2003) Nature and role of natural alteration gels formed on the surface of ancient volcanic glasses (Natural analogs of waste containment glasses). *J. Nucl. Mater.* **321**, 91–109.

DeGroat-Nelson P. J., Cameron B. I., Fink J. H. and Holloway J. R. (2001) Hydrogen isotope analysis of rehydrated siclic lavas: implications for eruption mechanisms. *Earth Planet. Sci. Lett.* **185**, 331–341.

Dettinger M. P. and Quade J. (2015) Testing the analytical protocols and calibration of volcanic glass for the reconstruction of hydrogen isotopes in paleoprecipitation. In *Geodynamics of a Cordilleran Orogenic System: The Central Andes of Argentina and Northern Chile* (eds. P.G. DeCelles, M.N. Ducea, B. Carrapa, P.A. Kapp), Geological Society of America, vol. 212, pp. 261–276.

Dobson P. F., Epstein S. and Stolper E. M. (1989) Hydrogen isotope fractionation between coexisting vapor and silicate glasses and melts at low pressure. *Geochim. Cosmochim. Acta* **53**, 2723–2730.

Eerkens J. W., Vaughn K. J., Carpenter T. R., Conlee C. A., Grados M. L. and Schreiber K. (2008) Obsidian hydration dating on the south coast of Peru. *J. Archaeol. Sci.* **35**, 2231–2239.

Ferrand K., Abdelouas A. and Grambow B. (2006) Water diffusion in the simulated French nuclear waste glass SON 68 contacting silica rich solutions: experimental and modeling. *J. Nucl. Mater.* **355**, 54–67.

Fontijn K., Ernst G. G. J., Elburg M. A., Williamson D., Abdallah E., Kwelwa S., Mbede E. and Jacobs P. (2010) Holocene explosive eruptions in the Rungwe Volcanic Province, Tanzania. *J. Volcanol. Geoth. Res.* **196**, 91–110.

Fontijn K., Lachowycz S. M., Rawson H., Pyle D. M., Mather T. A., Naranjo J. A. and Moreno-Roa H. (2014) Late Quaternary tephrostratigraphy of southern Chile and Argentina. *Quatern. Sci. Rev.* **89**, 70–84.

Friedman I., Smith R. L. and Long W. D. (1966) Hydration of natural glass and formation of perlite. *Geol. Soc. Am. Bull.* **77**, 323–328.

Friedman I., Gleason J., Sheppard R. A. and Gude A. J. (1993a) Deuterium fractionation as water diffuses into silicic volcanic ash. *Geophys. Monogr.* **78**, 321–323.

Friedman I., Gleason J. and Warden A. (1993b) Ancient climate from deuterium content of water in volcanic glass. *Geophys. Monogr.* **78**, 309–319.

Giachetti T. and Gonnermann H. M. (2013) Water in volcanic pyroclast: rehydration or incomplete degassing? *Earth Planet. Sci. Lett.* **369–370**, 317–332.

Giachetti T., Gonnermann H. M., Gardner J. E., Shea T. and Gouldstone A. (2015) Discriminating secondary from magmatic water in rhyolitic matrix-glass of volcanic pyroclasts using thermogravimetric analysis. *Geochim. Cosmochim. Acta* **148**, 457–476.

Gin S., Ryan J. V., Schreiber D. K., Neeway J. and Cabié M. (2013) Contribution of atom-probe tomography to a better understanding of glass alteration mechanisms: application to a nuclear glass specimen altered 25 years in a granitic environment. *Chem. Geol.* **349–350**, 99–109.

Henderson A. K., Nelson D. M., Hu F. S., Huang Y., Shuman B. N. and Williams J. W. (2010) Holocene precipitation seasonality captured by a dual hydrogen and oxygen isotope approach at Steel Lake, Minnesota. *Earth Planet. Sci. Lett.* **300**, 205–214.

Ihinger P. D., Zhang Y. and Stolper E. M. (1999) The speciation of dissolved water in rhyolitic melt. *Geochim. Cosmochim. Acta* **63**, 3567–3578.

Jezek P. A. and Noble D. C. (1978) Natural hydration and ion exchange of obsidian: an electron microprobe study. *Am. Mineral.* **63**, 266–273.

Kyle P. R., Ponomareva V. V. and Chluep R. R. (2011) Geochemical characterization of marker tephra layers from major Holocene eruptions, Kamchatka Peninsula, Russia. *Int. Geol. Rev.* **53**, 1059–1097.

Mazer J. J., Stevenson C. M., Ebert W. L. and Bates J. K. (1991) The experimental hydration of obsidian as a function of relative humidity and temperature. *Am. Antiq.* **56**, 504–513.

Mulch A., Sarna-Wojcicki A. M., Perkins M. E. and Chamberlain C. P. (2007) A Miocene to Pleistocene climate and elevation record of the Sierra Nevada (California). *Proc. Natl. Acad. Sci.* **105**(19), 6819–6824.

Newman S., Stolper E. M. and Epstein S. (1986) Measurement of water in rhyolitic glasses: calibration of an infrared spectroscopic technique. *Am. Mineral.* **71**, 1527–1541.

Newman S., Epstein S. and Stolper E. (1988) Water, carbon dioxide, and hydrogen isotopes in glasses from the ca. 1340 A. D. eruption of the Mono Craters, California: constraints on degassing phenomena and initial volatile content. *J. Volcanol. Geoth. Res.* **35**(1–2), 75–96.

Nolan G. S. and Bindeman I. N. (2013) Experimental investigation of rates and mechanisms of isotope exchange (O, H) between volcanic ash and isotopically-labeled water. *Geochim. Cosmochim. Acta* **111**, 5–27.

Oelkers E. H. (2001) General kinetic description of multioxide silicate mineral and glass dissolution. *Geochim. Cosmochim. Acta* **65**, 3703–3719.

Parruzot B., Jollivet P., Rébiscoul D. and Gin S. (2015) Long-term alteration of basaltic glass: mechanisms and rates. *Geochim. Cosmochim. Acta* **154**, 28–48.

Ponomareva V., Kyle P. R., Melekestsev I. V., Rinkleff P. G., Dirksen O. V., Sulerzhitksy L. D., Zaretskaia N. E. and Rourke R. (2004) The 7600 (^{14}C) year BP Kurile Lake caldera-forming eruption, Kamchatka, Russia: stratigraphy and field relationships. *J. Volcanol. Geoth. Res.* **136**, 199–222.

Ponomareva V., Melekestev I., Braitseva O., Churikova T., Pevzner M. and Sulerzhitsky L. (2007) Late Pleistocene-Holocene volcanism on the Kamchatka Peninsula, Northwest Pacific Region. In *Volcanism and Subduction: The Kamchatka Region* (eds. J. Eichelberger, E. Gordeev, M. Kasahara, P. Izbekov, J. Lees), American Geophysical Union, Geophysical Monograph 172, 165–198.

Ponomareva V., Portnyagin M., Derkachev A., Pendea I. F., Bourgeois J., Reimer P. J., Garbe-Schönberg D., Krasheninnikov S. and Nürnberg D. (2013) Early Holocene M∼6 explosive eruption from Plosky volcanic massif (Kamchatka) and its tephra as a link between terrestrial and marine paleoenvironmental records. *Int. J. Earth Sci.* **102**, 1673–1699.

Princen H. (1979) Highly concentrated emulsions. I. Cylindrical systems. *J. Colloid Interface Sci.* **71**, 55–66.

Proussevitch A. A., Sahagian D. L. and Anderson A. T. (1993) Dynamics of diffusive bubble growth in magmas: isothermal case. *J. Geophys. Res.* **98**, 22283–22307.

Qi H., Gröning M., Coplen T. B., Buck B., Mroczkowski S. J., Brand W. A., Geilmann H. and Gehre M. (2010) Novel silver-tubing method for quantitative introduction of water into high-temperature conversion systems for stable hydrogen and oxygen isotopic measurements. *Rapid Commun. Mass Spectrom.* **24**, 1821–1827.

Qi H., Coplen T. B., Olack G. A. and Vennemann T. W. (2014) Caution on the use of NBS 30 biotite for hydrogen-isotope measurements with on-line high-temperature conversion systems. *Rapid Commun. Mass Spectrom.* **28**, 1987–1994.

Rébiscoul D., Rieutord F., Né F., Frugier P., Cubitt R. and Gin S. (2007) Water penetration mechanisms in nuclear glasses by X-ray and neutron reflectometry. *J. Non-Cryst. Solids* **353**, 2221–2230.

Riciputi L. R., Elam J. M., Anovitz L. M. and Cole D. R. (2002) Obsidian diffusion dating by secondary ion mass spectrometry: a test using results from Mound 65, Chalco, Mexico. *J. Archaeol. Sci.* **29**(10), 1055–1075.

Ross C. S. and Smith R. L. (1955) Water and other volatiles in volcanic glasses. *Am. Mineral.* **40**, 1071–1089.

Rust A. C. and Cashman K. V. (2011) Permeability controls on expansion and size distributions of pyroclasts. *J. Geophys. Res.* **116**, 1–17.

Sarna-Wojcicki A. M. and Davis J. O. (1991) Quaternary tephrochronology. In *Quaternary nonglacial geology–conterminous U.S.* (eds. R. B. Morrison), Geological Society of America, Geology of North America K2, 93–116.

Shane P. and Ingraham N. (2002) δD values of hydrated volcanic glass: a potential record of ancient meteoric water and climate in New Zealand. *NZ J. Geol. Geophys.* **45**(4), 453–459.

Silver L. A., Ihinger P. D. and Stolper E. (1990) The influence of bulk composition on the speciation of water in silicate glasses. *Contrib. Mineral. Petrol.* **104**, 142–162.

Steefel C. I., Beckingham L. E. and Landrot G. (2015) Micro-continuum approaches for modeling pore-scale geochemical processes. *Rev. Mineral. Geochem.* **80**, 217–246.

Stroncik N. A. and Schmincke H. (2002) Palagonite – a review. *Int. J. Earth Sci.* **91**, 680–697.

Tuffen H., Owen J. and Denton J. S. (2010) Magma degassing during subglacial eruptions and its use to reconstruct palaeo-ice thicknesses. *Earth Sci. Rev.* **99**, 1–18.

Valle N., Verney-Carron A., Sterpenich J., Libourel G., Deloule E. and Jollivet P. (2010) Elemental and isotopic (^{29}Si and ^{18}O) tracing of glass alteration mechanisms. *Geochim. Cosmochim. Acta* **74**, 3412–3431.

Zhang Y. (1999) H_2O in rhyolitic glasses and melts: measurement, speciation, solubility, and diffusion. *Rev. Geophys.* **37**, 493–516.

Zhang Y. and Behrens H. (2000) H_2O diffusion in rhyolitic melts and glasses. *Chem. Geol.* **169**, 243–262.

Associate editor: Carl Steefel